Evidence from combined analysis of single cell RNA-Seq and ATAC-Seq data of regulatory toggles operating in native and iPS-derived murine retina

Anouk Georges[1,2], Arnaud Lavergne[4], Michiko Mandai[5], Fanny Lepiemme[1], Latifa Karim[4], Loic Demeulenaere[3], Diego Aguilar[3], Michael Schyns[6], Sébastien Dupont[3], Laurent Nguyen[1], Jean-Marie Rakic[2], Masayo Takahashi[7], Michel Georges[3$] & Haruko Takeda[3].

[1]GIGA Stem Cells, GIGA Institute, University of Liège, Belgium. [2]Department of Ophthalmology, Faculty of Medicine and CHU University Hospital, University of Liège, Belgium. [3]GIGA Medical Genomics, GIGA Institute, University of Liège, Belgium. [4]GIGA Genomics Platform, GIGA Institute, University of Liège, Belgium. [5]Laboratory for Retinal Regeneration, Center for Developmental Biology, RIKEN, Japan. [6]Digital Business, HEC Management School, University of Liège, Belgium. [7]Senior Visiting Scientist, Laboratory for Retinal Regeneration, Center for Biosystems Dynamics Research, RIKEN, Japan.

[$]Corresponding author: michel.georges@uliege.be

Abstract

We report the generation and analysis of single-cell RNA-Seq data (> 38,000 cells) from native and iPSC-derived murine retina at four matched developmental stages spanning the emergence of the major retinal cell types. We combine information from temporal sampling, visualization of 3D UMAP manifolds, pseudo-time and RNA velocity analyses, to show that iPSC-derived 3D retinal aggregates broadly recapitulate the native developmental trajectories. However, we show relaxation of spatial and temporal transcriptome control, premature emergence and dominance of photoreceptor precursor cells, and susceptibility of dynamically regulated pathways and transcription factors to culture conditions in iPSC-derived retina. We generate bulk ATAC-Seq data for native and iPSC-derived murine retina identifying ~125,000 peaks. We combine single-cell RNA-Seq with ATAC-Seq information and obtain evidence that approximately half the transcription factors that are dynamically regulated during retinal development may act as repressors rather than activators. We propose that sets of activators and repressors with cell-type specific expression constitute "regulatory toggles" that lock cells in distinct transcriptome states underlying differentiation. We provide evidence supporting our hypothesis from the analysis of publicly available single-cell ATAC-Seq data for adult mouse retina. We identify subtle but noteworthy differences in

the operation of such toggles between native and iPSC-derived retina particularly for the Etv1, Etv5, Hes1 and Zbtb7a group of transcription factors.

Keywords: retina, iPSC, single-cell RNA-Seq, ATAC-Seq, transcription factor

Introduction

It has recently become possible to recapitulate retinal development from induced pluripotent stem cells (iPSCs) in human and mice [1-3]. This has opened new avenues to explore the molecular mechanisms underlying developmental competence, commitment and differentiation for each of the major cell types during retinal neurogenesis. It offers hope to improve therapies for retinal degenerative diseases which afflict tens of millions of people in the US and Europe alone and may account for approximately 50% of all cases of blindness [4]. Stem cells derived from patient-specific somatic cells offer new opportunities to study the effects of gene defects on human retinal development in vitro and to test small molecules or biologics to treat the corresponding disorders [5,6].

Assessing how faithfully iPSC-derived 3D retinal aggregates recapitulate specific developmental programs has typically been done by monitoring the expression of limited numbers of cell-type specific markers and examining the spatial patterning of the corresponding groups of cells [7]. Interrogating the expression of a handful of marker genes/proteins does not fully inform about the proper temporal and spatial execution of the epigenetic program, nor does it inform about the presence of aberrant cell types. Single-cell RNA-sequencing (scRNA-Seq) now enables the profiling of samples of the transcriptome (typically between 3% and 15% of mRNAs present in a cell depending on the methodology) of individual cells. This permits the clustering of cells based on the similarity of their transcriptome and the identification of cellular subtypes including some that may not have been recognized before [8]. It allows to refine developmental trajectories by identifying cells occupying intermediate states connecting clusters in multidimensional expression space [9,10] and by predicting the developmental orientation taken by individual cells based on measured deviations from the steady-state ratio between spliced and unspliced RNA molecules (“RNA velocity”) [11,12]. Genes that are defining cellular sub-types can be pinpointed by differential expression analysis between clusters [13], while genes that drive the differentiation process may be identified by searching for gene sets that are dynamically

64 regulated across real and/or pseudo-time [14]. Recently, scRNA-Seq has been used to
65 compare transcriptome dynamics during native and embryonic stem cells (ESC)- or iPSC-
66 derived retinal development in human [15-17]. This has revealed comparable cellular
67 composition at equivalent ages and the convergence of the organoid transcriptomes to that
68 of adult peripheral retinal cell types with, however, some differences in gene expression of
69 particular cell types as well as structural differences of inner retinal lamination that seems
70 disrupted in advanced organoid stages compared with fetal retina [16]. It has revealed striking
71 cell type-specific expression of genes underpinning inherited diseases such as Leber
72 congenital amaurosis, retinitis pigmentosa, stationary night blindness and achromatopsia,
73 and its conservation in organoids [17].
74 Here we report the generation and use of scRNA-Seq data collected at four matched stages
75 of native and iPSC-derived retinal development in the mouse to study the dynamics of the
76 transcriptome and compare it between the two systems. We integrate scRNA-Seq data with
77 bulk and single-cell ATAC-seq data (which identify active gene regulatory elements by virtue
78 of local chromatin openness [18]), and provide evidence for the operation of transcription
79 factor (TF)-based regulatory toggles combining activators and repressors, that may lock the
80 transcriptome of distinct cellular sub-types in both native and iPSC-derived retina thereby
81 underpinning the different cellular identities.
82

83 **Results**

84 ***Joint analysis of scRNA-Seq data from native retina and iPSC-derived 3D retinal aggregates***
85 ***highlights canonical cell types and developmental trajectories.***

86 To contribute to the comparison of the developmental trajectories in native retina (NaR) and
87 iPSC-derived 3D retinal aggregates (3D-RA), we performed scRNA-Seq of murine NaR and 3D-
88 RA at four matched stages of development: embryonic day (E)13 vs differentiation day
89 (DD)13, postnatal day (P)0 vs DD21, P5 vs DD25 and P9 vs DD29 [19]. NaR were dissected
90 from two to 11 C57BL/6 mice (of both sexes) per stage. Mouse 3D-RA were generated from
91 the Nrl-GFP (C57BL/6 background) iPSC line [20] following [21-22] (SFig. 1). Optic vesicle-like
92 structures (OV) were manually dissected from 3D-RA. Cells from NaR and OV were dissociated
93 and subjected to droplet-based scRNA-Seq using a 10X Genomics Chromium platform. We
94 obtained sequence information for 21,249 cells from NaR and 16,842 cells from 3D-RA,
95 distributed evenly amongst developmental stages. We generated an average of 74,808 reads

96 per cell, corresponding to 5,940 unique molecular identifiers (UMIs) and 2,471 genes per cell
97 (STable 1).

98 We first analyzed all data jointly (i.e. NaR and 3D-RA) to cover a maximum of intermediate
99 developmental stages and hence generate the most continuous manifold possible. We used
100 Canonical Correlation Analysis (CCA) implemented with Seurat [23] to align the NaR and 3D-
101 RA datasets based on the expression profiles of 1,253 "most variable" genes (STable 2). We
102 projected the corresponding 30-dimensional distances (based on the 30 first CCA) between
103 cells in 2D- and 3D-space using Uniform Manifold Approximation and Projection (UMAP) [24].
104 We assigned all 38,091 cells jointly (i.e. NaR and 3D-RA) to 71 clusters by k-means clustering
105 (Fig. 1A).

106 We defined gene expression signatures for 13 recognized retinal cell types using published
107 information [25] (STable 3 and SFig. 2), and regrouped the clusters accordingly in 13 cell types
108 corresponding to neuroepithelium (NE), retinal pigmented epithelium (RPE), early (ERPC), late
109 (LRPC), and neurogenic retinal progenitor cells (NRPC), retinal ganglion cells (RGC), horizontal
110 cells (HC), amacrine cells (AC), photoreceptor precursor cells (PRP), cones (C), rods (R), bipolar
111 cells (BC), and Müller cells (MC) (Fig. 1B). Using additional gene expression signatures we
112 further identified: (i) actively dividing ERPC, LRPC and NRPC (in S and G2-M phases of the cell
113 cycle)[26], (ii) T1, T2 and T3 post-mitotic transitional precursor cell populations recognized in
114 human native and hPSC-derived retina [16], (iii) the ciliary marginal zone (CMZ) [27], (iv) a
115 recently described subgroup of Tbr1^{+} RGC cells located in the inner plexiform layer [28], and
116 (v) starburst AC [29](Fig. 1C, SFig. 2 and STable 3).

117 Labelling cells by developmental stage (stages I to IV) distinguished ERPC from LRPC, and
118 revealed the expected sequence of emergence of RGC (stage I), followed by HC, AC and PRP
119 (stage II and III), then C, R, BC and MC (stage III and IV). Cells assigned to the Tbr1+ RGC cluster
120 appeared at stage II and III. T1, T2 and T3 cells appeared in that order, and starburst AC at
121 stage II and III (Fig. 1D). The UMAP manifold connected cell types consistently with known
122 developmental trajectories [16,25,30,31], including: (i) NE -> RPE, (ii) NE -> ERPC, (iii) ERPC ->
123 NRPC (T1) -> RGC, (iv) LRPC -> NRPC (T1->T2) -> AC, (v) LRPC -> NRPC (T1) -> PRP (T3) -> C/R,
124 and (vi) LRPC -> MC. Reminiscent of previous studies [16,25], the cluster of HC cells was
125 disconnected from the rest of the manifold providing no information about their precursors.
126 In agreement with [25], BC appeared to emerge from PRP cells distinct from NRPC or T3

(Suppl. Video: http://www.sig.hec.ulg.ac.be/giga). Cell-specific RNA velocities [11] were consistent with the ERPC -> NRPC -> RGC trajectory but otherwise difficult to interpret (Fig. 1E). However, velocity pseudotime analysis (using a velocity-inferred transition matrix) implemented with scvelo [12] was remarkably proficient at ordering the four stages of development, as well as at identifying terminal cellular states (without benefitting from any information about development stage or root cells)(Fig. 1F).

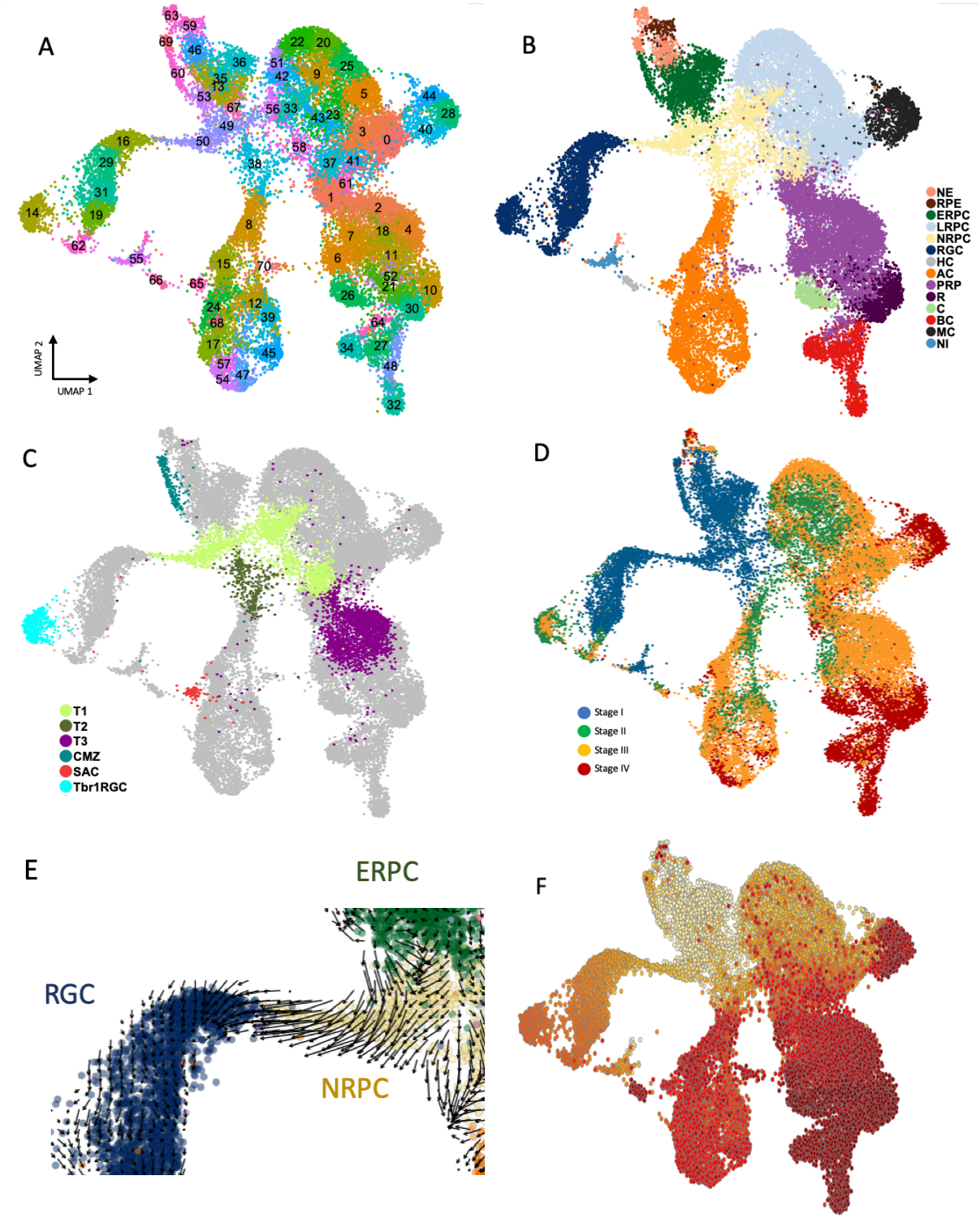

149 **Figure 1: Joint scRNA-Seq-based UMAP of 38,091 cells corresponding to four developmental stages of native**
150 **(NaR) and iPS-derived (3D-RA) murine retina. (A)** 2D UMAP manifold showing NaR and 3D-RA cells jointly and
151 their assignment to 71 clusters by k-means clustering. **(B)** Merging of the clusters in 13 major retinal cell types
152 corresponding to neuroepithelium (NE), retinal pigmented epithelium (RPE), early (ERPC), late (LRPC),
153 neurogenic retinal progenitor cells (NRPC), retinal ganglionic cells (RGC), horizontal cells (HC), amacrine cells
154 (AC), photoreceptor precursor cells (PRP), cones (C), rods (R), bipolar cells (BC), and Müller cells (MC), on the
155 basis of the expression of known marker genes (SFig. 2). **(C)** Identifying known retinal sub-populations: post-
156 mitotic transitional precursor cell populations (T1, T2, T3)[16], Ciliary Marginal Zone (CMZ)[27], Tbr1+ retinal
157 ganglionic cells (Trb1RGC)[28], and starburst amacrine cells (SAC)[29]. **(D)** Cells colored by developmental stage:
158 I. blue = DD13 + E13, II. green = DD21 + P0, III. orange = DD25 + P5, IV. red = DD29 + P9. **(E)** Cell-specific RNA
159 velocities [11] confirming the ERPC -> NRPC (T1) -> RGC cellular trajectory. **(F)** Velocity pseudo-time analysis
160 using a velocity-inferred transition matrix [12]. Increase in pseudo-time is marked by increase in redness.
161

162 ***Comparison of NaR and 3D-RA cell fates in UMAP space highlights commonalities and***
163 ***differences in developmental trajectories.***

164 We then focused on the comparison between the behavior of NaR and 3D-RA cells. Global
165 comparison of the distribution of NaR and 3D-RA cells across the manifold indicates that in
166 vitro neuro-retinal differentiation from iPSCs largely recapitulates native development (Fig.
167 2A). This is substantiated by noting that 82% of the 71 clusters and 86% of the 13 cell types
168 contain at least 10% of the least represented cell origin (NaR or 3D-RA) (Fig. 2B&C).
169 More granular examination, however, reveals noteworthy differences. The first one is the
170 occurrence of NaR- or 3D-RA specific clusters and cell types: (i) the RPE cell type is almost
171 exclusively composed of 3D-RA cells as a result of RPE elimination from NaR by dissection; (ii)
172 the CMZ is absent in 3D-RA (only recently were culture conditions established for inducing
173 selective CM retinal differentiation in human iPSC-derived RA [32]); (iii) AC cluster 65, thought
174 to correspond to starburst AC, was only observed in 3D-RA; (iv) BC clusters 32, 34 and 48 are
175 nearly exclusively composed of NaR cells, and (v) cluster 55 is exclusively populated by 3D-RA
176 cells. Cluster 55 is thought to result from aberrant in vitro differentiation of NE into non-
177 retinal neuronal cells. Indeed, it is connected to NE by a cellular bridge (Video:
178 http://www.sig.hec.ulg.ac.be/giga), and strongly expresses Tbr1 and other genes typical of
179 developing cortical neurons including reelin (STable 4&6). It is therefore
180 The second difference is the apparent relaxation of pseudo-spatial and pseudo-temporal
181 transcriptome control in 3D-RA versus NaR. The developmental pathways traversed by NaR
182 cells indeed appear tighter than those of 3D-RA cells, while NaR cells sampled at a specific
183 developmental stage seem to populate fewer cell types than 3D-RA cells. To quantify the
184 former, we down-sampled cells to equalize NaR and 3D-RA numbers (within developmental
185 stage) and computed the average distance from the *n* closest neighbors, which was indeed

186 highly significantly shorter for NaR than for 3D-RA (Fig. 2D). To quantify the latter, we
187 measured the diversity of cell types within stages (using a measure of entropy), which was
188 indeed significantly lower in NaR than in 3D-RA for all four stages (Fig. 2E). The last
189 noteworthy differences between both systems is the observation that PRP arise earlier in 3D-
190 RA than in NaR and accumulate at the expense of other cell types (particularly LRPC), yet
191 partially fail terminal differentiation particularly into BC cells (Fig. 2A&F).

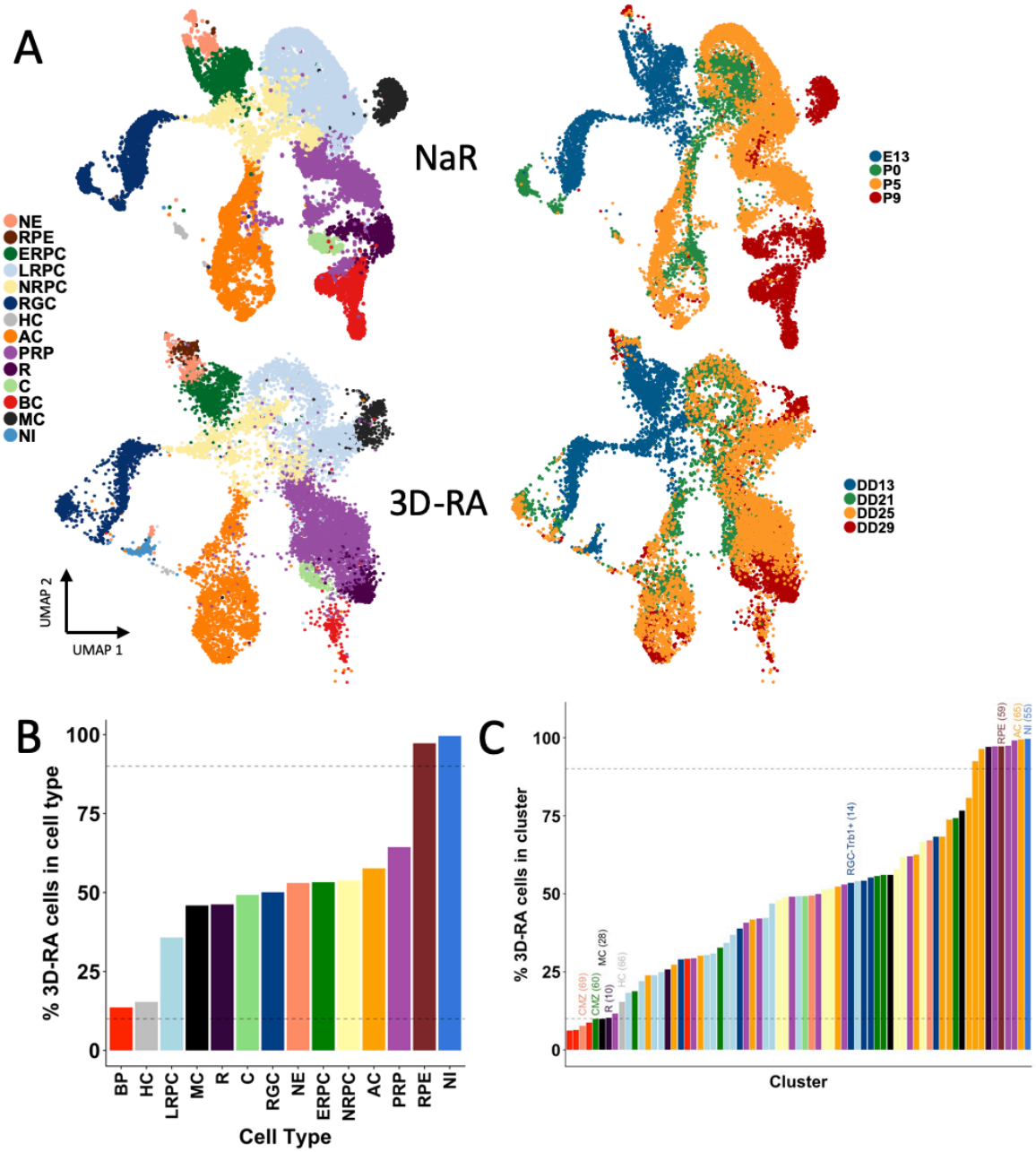

192
193

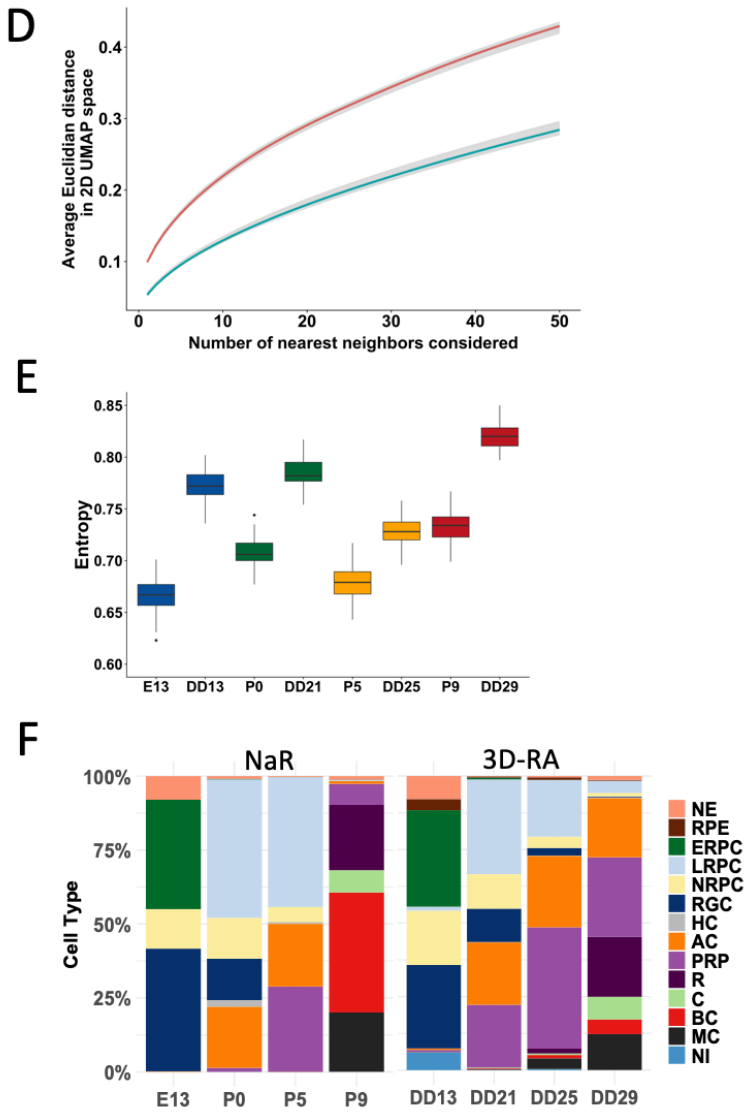

Figure 2: Comparison of Nar and 3D-RA cells in scRNA-Seq-based UMAP space. (A) Distribution of NaR (upper) versus 3D-RA (lower) cells across the UMAP manifold, sorted by cell type (left) and developmental stage (right). **(B-C)** Proportion of 3D-RA cells (adjusted for number of NaR and 3D-RA cells) in 14 cell types (B) and 71 clusters (C). 86% of cell types and 82% of clusters contain at least 10% of the least represented cell origin (NaR vs 3D-RA). Cell types are colored as in (A) and clusters are colored according to the cell type to which they were assigned. Notable clusters discussed in the main text are highlighted. Cluster 65 corresponds presumably to starburst AC. **(D)** Larger average distance in 2D UMAP space (Y-axis) from *n* nearest neighbors (X-axis) for 3D-RA (red) than for NaR cells (blue). **(E)** Larger cell type diversity (sampling-based measure of entropy) in the four developmental stages for 3D-RA than for NaR. **(F)** Proportions of cell types within developmental stage for NaR (left) and 3D-RA (right).

3D-RA culture conditions perturb genes and pathways that play key roles in NaR development.

To identify key genes for retinal differentiation, we performed differential expression analysis for each cell type against all others, first considering NaR cells only. In NaR, we identified a total of 4,177 genes with significantly higher expression in at least one of the 13 main cell-types (as defined above) compared to all other cell types merged (log-fold change ≥ 0.25 and p-value ≤ 0.001), hereafter referred to as "cell type-specifying" genes (Fig. 3A and STable 4). Of those, 3,675 were also identified as dynamically regulated genes when using Monocle 2 [14] (SFig. 3 and STable 5).

We then searched for enriched Reactome pathways [33,34] in the 13 lists of "cell type-specifying" genes. Two hundred sixty-eight pathways were significantly enriched ($q \leq 0.01$)

237 in at least one cell-type (STable 6). These corresponded primarily to: (i) accelerated cell
238 division in ERPC, LRPC and NRPCs, (ii) intense post-transcriptional and translational activity in
239 NE, ERPC, LRPC and NRPCs, (iii) activation of RHO GTPase- and NOTCH-dependent signaling in
240 ERPC, LRPC, NRPCs, RGC and LRPC, NRPCs, respectively, as well as the GPCR-dependent
241 phototransduction cascade in C and R, (iv) activation of mitochondrial citric acid (TCA) cycle
242 and respiratory electro transport in HC, C, R, BC, and MC, of cholesterol synthesis in ERPC and
243 RGC, and of insulin- and glucagon-dependent metabolic integration in RGC and AC, (v)
244 enhanced remodeling of the extracellular matrix in NE, RPE and MC, and GAP junction
245 trafficking in RGC, and (vi) activation of ROBO receptors-dependent axon guidance in NE,
246 ERPC and LRPC, and of synapse formation in RGC, HC, AC and BC (Fig. 3B).
247 A Reactome pathway is considered enriched (in a list of submitted genes) if the number of
248 genes in the list that are part of the pathway (the number of "found-entities") is higher than
249 expected by chance alone [33,34]. The found-entities for different enriched Reactome
250 pathways often show considerable overlap. As an example, the same six genes
251 (*Rfc5;Rfc4;Rfc1;Rfc2;Prim1*) in the list of 465 ERPC-specifying genes explain the enrichment of
252 the "Leading strand synthesis" and "Polymerase switching" Reactome pathways (STable 6).
253 We devised a method to assign colors to sets of found-entities such that strongly overlapping
254 sets would have similar colors, while non-overlapping sets would have distinct colors
255 (Methods and SFig. 4). As an example, we can see from Fig. 3B that the 48 Reactome
256 pathways highlighted in NE correspond to six distinct sets of found entities (six dominant
257 colors), that one of these sets is also driving Reactome pathway enrichment in RPE (bordeau),
258 and that two others (indigo blue and purple) are also driving pathway enrichment in ERPC.
259
260 At first sight, genes that were differentially expressed between cell-types in NaR appeared to
261 recapitulate their in vivo expression profile quite well in 3D-RA (Fig. 3A). Yet, to better
262 appreciate the differences between in vivo and in vitro retinal differentiation, we performed
263 differential expression analysis between NaR and 3D-RA separately for each cell type. For
264 each of the 13 major cell types, we generated two lists of genes corresponding respectively
265 to genes that were under-expressed in 3D-RA when compared to NaR (NaR>3D-RA) and genes
266 that were over-expressed in 3D-RA when compared to NaR (3D-RA>NaR) ($q \leq 0.01$; STable
267 7). We then searched for biological pathways that were over-represented in the
268 corresponding gene lists using Reactome. This yielded 197 downregulated (NaR > 3D-RA) and

134 upregulated (3D-RA > NaR) pathways (Fig. 3B and STable 8). Strikingly, both down- and upregulated pathways (i.e. when comparing NaR and 3D-RA by cell type) exhibited considerable overlap with the pathways identified (see previous paragraph) when comparing cell types within NaR (Cell type > Others) (115/197, $p < 10^{-6}$ and 67/134, $p < 10^{-6}$) (Fig. 3C). More specifically, (i) the rate of cell division in NE, ERPC, LRPC and NRPC was reduced in 3D-RA when compared to NaR, (ii) post-transcriptional and translational mechanisms were exacerbated in ERPC, LRPC, NRPC, RGC, PRP, C, R, BC and MC of 3D-RA, when compared to NaR, (iii) signal transduction via WNT, TGF-beta, RHO GTPases, Esr, Notch, Hedgehog, MAPK, and Death receptors was diminished in 3D-RA when compared to NaR, particularly in ERPC and LRPC, while the phototransduction cascade was less active in 3D-RA-derived R than in NaR-derived R, (iv) mitochondrial citric acid (TCA) cycle and respiratory electron transport was increased in 3D-RA's LRPC, NRPC, AC, PRP and C (yet increased in BC), cholesterol synthesis increased in 3D-RA's C and R, and gluconeogenesis increased in 3D-RA's PCP and R, (v) stress response and apoptosis was reduced in 3D-RA's ERPC, yet increased in 3D-RA's C, R, BC and MC (i.e. at the latest stages of 3D-RA culture), and (vi) vesicle mediated transport and synapse formation was decreased in 3D-RA's LRPC, RGC and PRP (Fig. 3B). As testified by their assigned colors in Fig. 3B, the found-entities driving Reactome pathway enrichment when analyzing cell-type specifying genes (Cell type > Others) or when comparing NaR and 3D-RA (NaR > 3D-RA and 3D-RA > NaR) showed considerable overlap (see also SFig. 4). Thus, the genes and pathways that appear to be the most perturbed by the 3D-RA culture conditions are also the ones that play key roles in NaR development (i.e. the cell type-specifying genes as defined above).

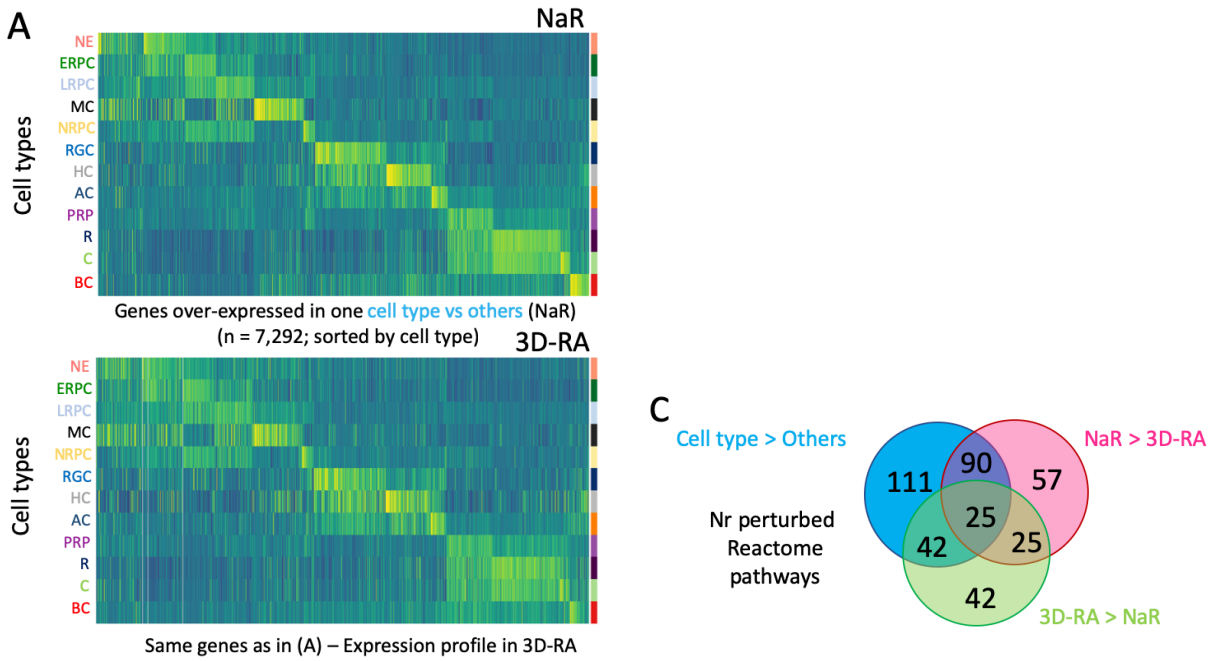

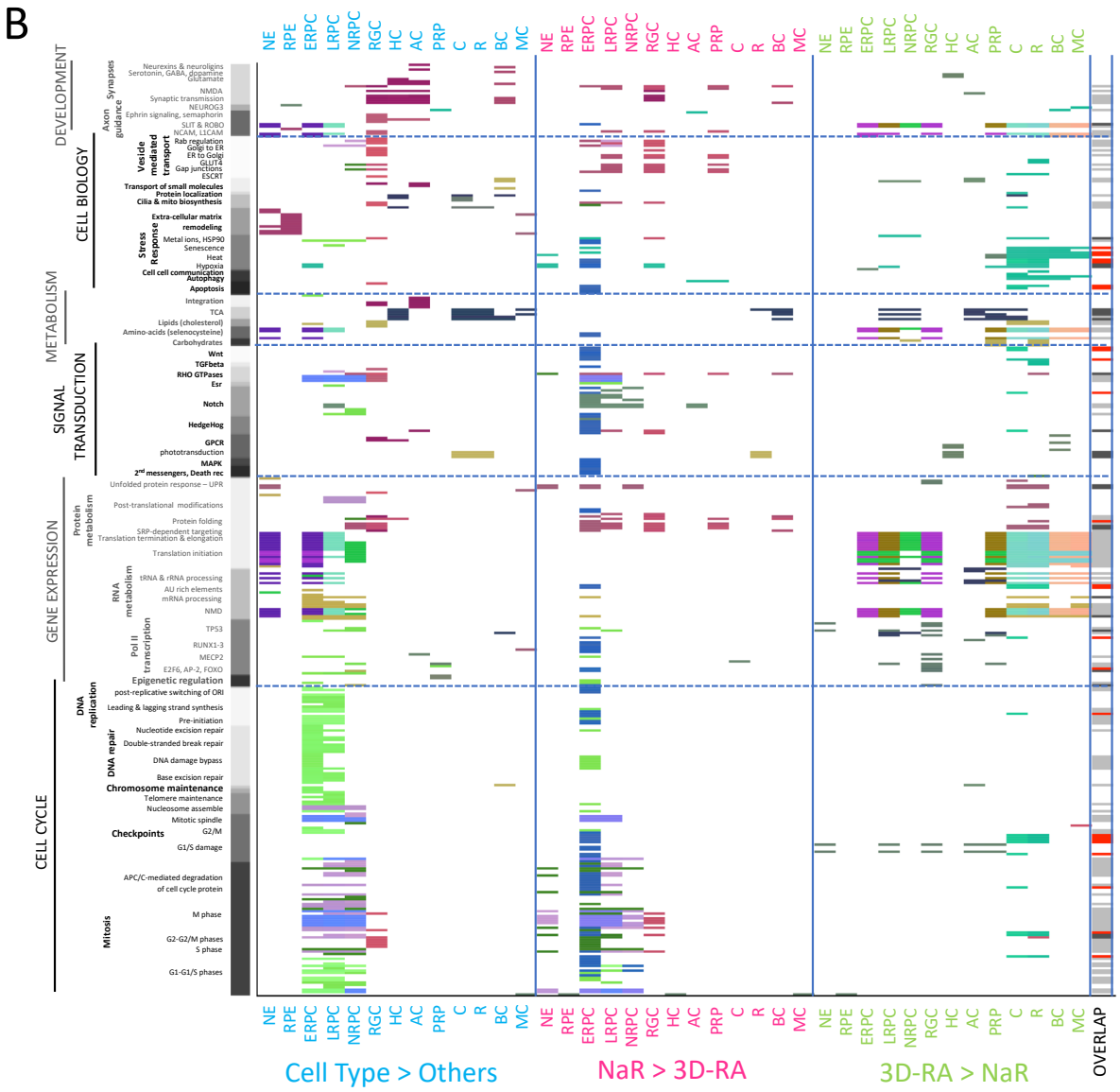

Figure 3: Comparison of the cell type-specific transcriptome of NaR and 3D-RA by means of scRNA-Seq. (A) Expression profiles in 12 cell types of 7,292 genes that are dynamically regulated during in vivo retinal development (i.e. significantly overexpressed in at least one cell type when compared to all other ones in NaR) in NaR (upper panel) and 3D-RA (lower panel). Abbreviations refer to cell types and are as defined in Fig. 1 (including color code). **(B)** Reactome pathways that are significantly ($p \leq 0.001$) enriched amongst differentially expressed genes ("Cell type > Other": when comparing expression levels between specific cell types and all other cells in NaR only; "NaR > 3D-RA" and "3D-RA > NaR": when comparing expression levels between NaR and 3D-RA cells within cell type). Y-axis: Reactome pathways sorted by "top level" system (cell cycle, gene expression, signal transduction, metabolism, cell biology and development) and sub-level therein. Tiles mark the pathways that are significantly enriched in the corresponding contrast and cell type. The colors of the tiles reflect similarity in "found entities" as described in the main text and SFig. 4. Last column ("Overlap"): White: pathways significant in one contrast only, Black: pathways significant in all three contrasts, Grey: pathways significant in "Cell type > Other" and ("NaR > 3D-RA" or "3D-RA > NaR"), Red: pathways significant in "NaR > 3D-RA" and "3D-RA > NaR". **(C)** Number of unique and shared Reactome pathways between "Cell type > Other", "NaR > 3D-RA" and "3D-RA > NaR". All overlaps are highly significant ($p < 10^{-6}$) assuming random sampling from 2,365 Reactome pathways.

310 ***The expression level of many transcription factors is perturbed in 3D-RA.***

311 The 4,177 cell type-specifying genes in NaR (i.e. Cell type > Others, cfr above) comprised 293
312 transcription factors (TF)[35], including 107 that were at least 1.5 times more strongly
313 expressed in one cell type when compared to any of the other cell types (Fig. 4A and STable
314 4). The latter comprised 88 TF that were previously reported in the context of retinal
315 development, as well as 19 novel ones (NE: Peg3; LRPC: Lrrfip1; MC: Creb3l2, Csrnp1, Dbp,
316 Nr4a1, Nr4a3; HC: Zfp618, Zfp804a; AC: Zfp503; PRP: Foxo3, Lcorl; R: Zfp516, Trps1, Ppard,
317 Zc3h3, Mier1, Mier2, Lyar; BC: St18) (STable 9). Contrary to the overall expression profile (Fig.
318 3A), visual examination of the expression profiles of the 104 most differentially expressed TF
319 indicated considerable loss of cell-type specificity in 3D-RA (Fig. 4A). Indeed, 155 of the 293
320 (53%) differentially expressed TF were significantly ($q < 0.01$) under-expressed in at least one
321 cell type in 3D-RA when compared to NaR, while 80/293 (27%) were significantly ($q < 0.01$)
322 over-expressed in at least one cell type (Fig. 4B and SFig. 6). Striking examples include Skil
323 (ERPC), HevL (LRPC), Neurog2 (NRPC), Lhx1 (HC), Neurod2 (AC), Insm2 (PRP), Nfic (C/R), Ahr
324 (C/R), Bhlhe23 (BC) and Nr1d1 (MC), which are all significantly under-expressed in 3D-RA
325 when compared to NaR (Fig. 4C).
326 An additional 31 TF (not part of the
327 list of cell type-specifying genes)
328 were down-regulated in 3D-RA,
329 while 19 were upregulated (SFig.6).
330 Thus, the expression profile of a
331 remarkably high number of TF
332 appears perturbed in 3D-RA, and
333 this may in part drive the
334 differences observed between both
335 systems, including with regards to
336 Reactome pathways.
337

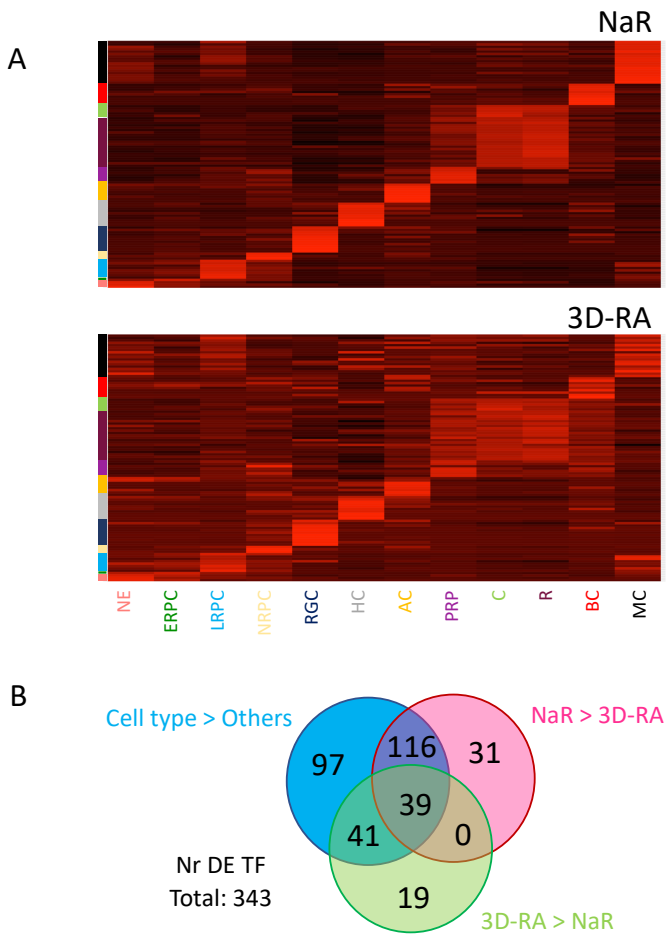

C

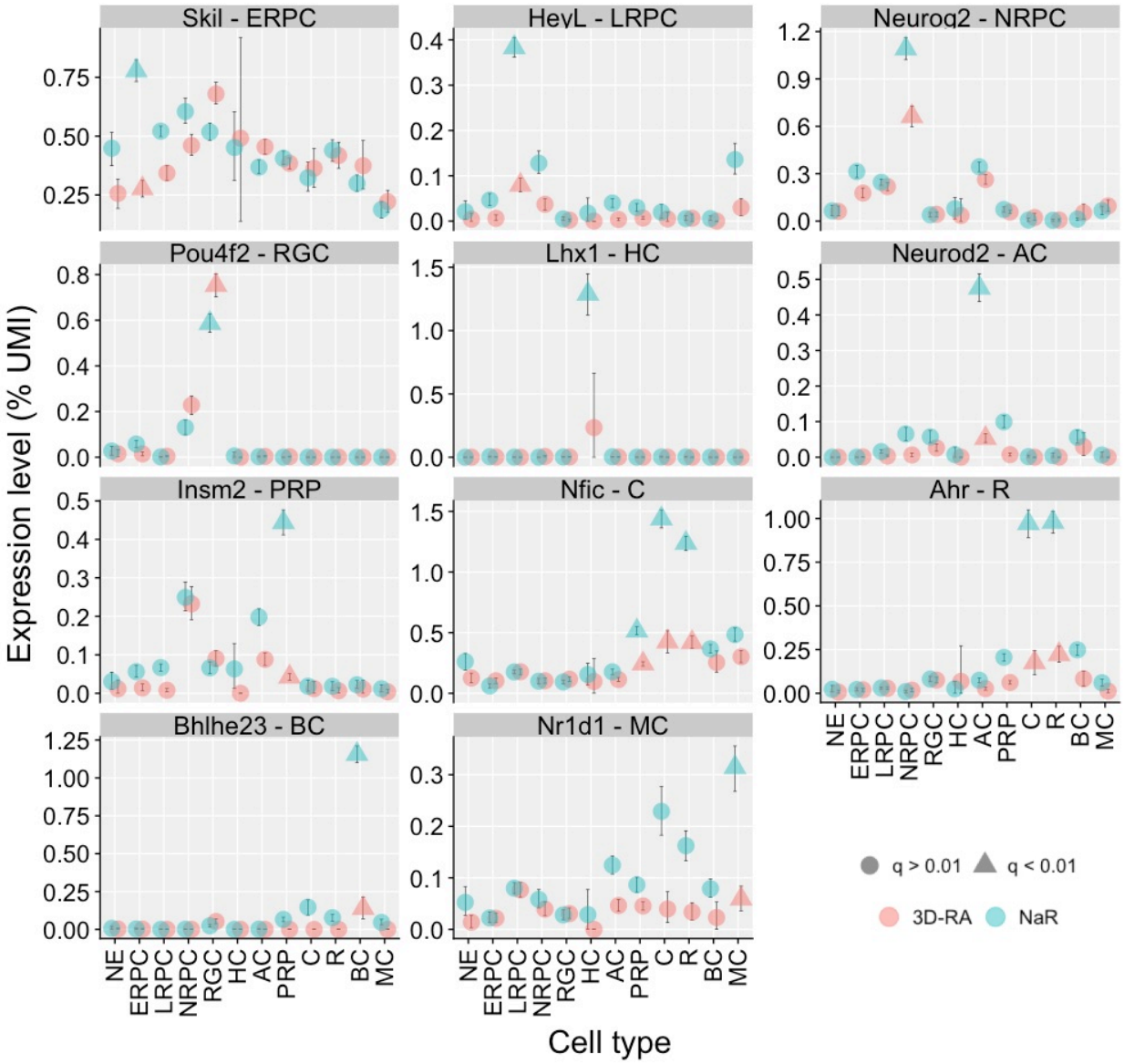

Figure 4: Comparison of the cell type-specific expression levels of TF in NaR and 3D-RA by means of scRNA-Seq. (A) Standardized expression levels of 104 most cell type-specific TF across 12 cell types in NaR (upper panel) and 3D-RA (lower panel). Abbreviations refer to cell types and are as defined in Fig. 1 (including color code). **(B)** Number of differentially expressed TF in "Cell type > Others", "NaR > 3D-RA", and "3D-RA > NaR", with corresponding overlaps. The overlaps are highly significant ($p < 10^{-6}$) assuming that TF are sampled randomly from the full collection of ~1,500 TFs [35]. **(C)** Examples of TF that are (i) significantly overexpressed in one cell type when compared to all others in NaR, and (ii) significantly under- or over-expressed in that cell type between NaR and 3D-RA. The average expression levels (fraction of UMI) of the corresponding genes in the different cell types are shown for NaR (green) and 3D-RA (red). The error bars correspond to 99% confidence intervals determined by bootstrapping (n=1000). Green triangles mark cell types in which the corresponding gene is significantly ($q < 0.01$, i.e. accounting for multiple testing) overexpressed in NaR when compared to all other cell types combined. Red triangles mark cell types in which the expression level differs significantly ($q < 0.01$) between NaR and 3D-RA. The gene name and cell type of interest are given in the facet headers.

353 ***Combined analysis of scRNA-Seq and bulk ATAC-Seq data reveals putative regulatory***
354 ***toggles in NaR.***
355 It is generally assumed that execution of the transcriptional program underlying
356 differentiation is controlled by dynamically regulated TF that activate downstream target
357 genes. To verify this assertion, we first performed bulk ATAC-Seq [36] on the first three stages
358 of NaR (E13, P0, P5) and 3D-RA (DD13, DD21, DD25) samples to identify gene-switch
359 components accessible during retinal development based on chromatin openness (SFig. 7A).
360 For each sample type, we analyzed two technical replicates of two biological replicates for a
361 total of 24 libraries. We defined a total of 123,482 peaks using MACS2 [37] (STable 10). Of
362 these, 93,386 (75.6%) were detected in NaR, 97,333 (78.8%) in 3D-RA. 18,933 (15.3%) were
363 common to all samples, 26,149 (30.0%) NaR-specific, 30,096 (24.4%) 3D-RA-specific, and
364 4,703 developmental stage-specific (3.8%; stage I: 294, stage II: 82, stage III: 4,327). The
365 number of peaks increased with developmental stage in NaR but not in 3D-RA (highest
366 number of peaks in DD13) (SFig. 7B). Nevertheless, stage I samples (E13 and DD13) clustered
367 together, while for subsequent stages samples clustered by origin (NaR vs 3D-RA) (SFig. 7C).
368 DNA binding motifs are reported for 151 of the TF found to be cell type-specifying by scRNA-
369 Seq (see above), amounting to a total of 336 motifs (average number of motifs per TF: 2.3;
370 range: 1 - 14). We used Homer to annotate our catalogue of ATAC-Seq peaks for the
371 corresponding motifs [38]. In total Homer identified 7,128,225 binding motifs in 98,181
372 ATAC-seak peaks assigned (based on closest proximity) to 19,171 genes (STable 11).
373 To test whether TF that were overexpressed in a given cell type were indeed activating
374 downstream target genes (as expected for “activator” TF), we searched for an enrichment of
375 the cognate binding motifs in the ATAC-Seq peaks of genes that were significantly over-
376 expressed in that cell type (relative to ATAC-Seq peaks of genes that were significantly under-
377 expressed in the same cell type). As an example, the Crx TF is overexpressed in PRP, C and R:
378 are ATAC-Seq peaks in the vicinity of the genes that are overexpressed in these cell types
379 enriched in Crx binding motifs as expected if Crx is an activator TF? We used average number
380 of binding motifs per ATAC-Seq peak per gene (total number of binding motifs divided by
381 number of peaks) as metric to correct for gene length. We first analyzed NaR, and found 84
382 instances of binding motif enrichment (q-value < 0.01) for 37 TF over-expressed in the
383 corresponding cell types (Fig. 5A, STable 12&13). Examples of such activator TF include Crx

384 (enrichment of all three known Crx binding motifs: Crx-1, Crx-2 and Crx-3) in PRP, R and C,
385 and Etv5 (1/1 binding motif) in LRPC (Fig. 5B).
386 Intriguingly, we observed 45 instances of binding motif depletion (q-value < 0.01) for 26 other
387 TF. Stated otherwise, for 26 TF that were over-expressed in a given cell type, binding motifs
388 were significantly more abundant in ATAC-Seq peaks of genes that were under-expressed
389 than in the ATAC-Seq peaks of genes that were over-expressed in the corresponding cell type
390 (Fig. 5A, STable 12&13). One explanation of this finding is that these TF act as repressors
391 rather than activators. Examples of such candidate "repressor" TF are Arh (1/2 binding
392 motifs) in C, and Tgif2 (2/3 binding motifs) in LRPC and NRPC (Fig. 5B).
393 We reasoned that such repressor TF may be components of regulatory toggles that ensure
394 cell type-specific gene expression not only by inducing expression of required genes (via
395 activator TF), but also by precluding expression of undesired genes (via repressor TF) (Fig. 5C).
396 To gain insights in the nature of the genes targeted by these putative repressor TF, we
397 searched for cell types in which the corresponding binding motifs were enriched in over-
398 expressed genes (even if the TF itself is not strongly expressed in that cell type). Fig. 5E shows
399 the corresponding results for all repressor TF over-expressed in a given cell type jointly. Thus,
400 for all candidate repressor TF identified in a given cell type (f.i. Foxp1, Nr2f1, Six6 and Sox2 in
401 ERPC; see Fig. 5E), we computed the log(1/p) value of the difference in the density of binding
402 motifs in over- versus under-expressed genes in each cell type, signed them according to the
403 direction of the difference (enrichment versus depletion in over-expressed genes), and
404 averaged these values across the (f.i. four in ERPC) candidate repressor TF. For comparison,
405 similar plots (Fig. 5D) are shown for the combined effect of all activator TF expressed in a
406 given cell type. This analysis revealed that the identified repressor TF systematically target
407 genes that are overexpressed in (and hence specify) another retinal cell type than the one(s)
408 in which they are expressed, with a clear pattern. It appears that the 12 cell types analyzed
409 in NaR form three clusters: (I) NE, ERPC, LRPC and NRPC, (II) RGC, AC and HC, and (III) PRP, C,
410 R, B, C and MC. Repressor TF which are expressed in cluster (I) are primarily targeting genes
411 that are over-expressed in cluster (III), repressor TF which are expressed in cluster (II) are
412 primarily targeting genes that are expressed in cluster (I) or (III), and repressor TF which are
413 expressed in cluster (III) primarily target genes that are expressed in cluster (I). There was
414 considerable overlap between the TF (activator and repressor) over-expressed in cell types

415 from the same cluster. As an example, Hif1A is over-expressed in R, C and BC (cluster III), while
416 Bahrl2 is over-expressed in RGC, AC and HC (cluster II)(Fig. 5E).
417 We also identified six "conditional activator" TF. These were characterized by the enrichment
418 of binding motifs in over-expressed genes for some cell type(s), yet the depletion of binding
419 motifs in over-expressed genes for other cell type(s) (Etv1, Fosb, Otx2, Pax6, Tcf3, Sox11) (Fig.
420 5B; STable 12&13). A good example is Otx2, which is significantly over-expressed in PRP and
421 NRPC, and whose three binding motifs are enriched in genes that are over-expressed in PRP
422 while being enriched in genes that are under-expressed in NRPC (which include the genes that
423 are over-expressed in PRP). One possible explanation of these observations is that the
424 corresponding TF are necessary but not sufficient to induce expression of target genes. As
425 an example, Otx2 may be induced in NRPC that will develop into PRP, but only exert its
426 transcriptional effects after maturation into PRP. Consistent with this hypothesis, NRPC
427 expressing Otx2 tended to cluster in the vicinity of PRP in the UMAP manifold (SFig. 8). We
428 therefore refer to these six TF as "conditional activators".
429 Finally, three TF were characterized by the enrichment of one of their binding motifs (in
430 overexpressed genes), yet the depletion of another of their binding motifs in the same cell
431 type (Lhx1, Plagl1, Zic1) (STable 12&13). These will be referred to as "dual TF" yet were
432 considered with caution.
433

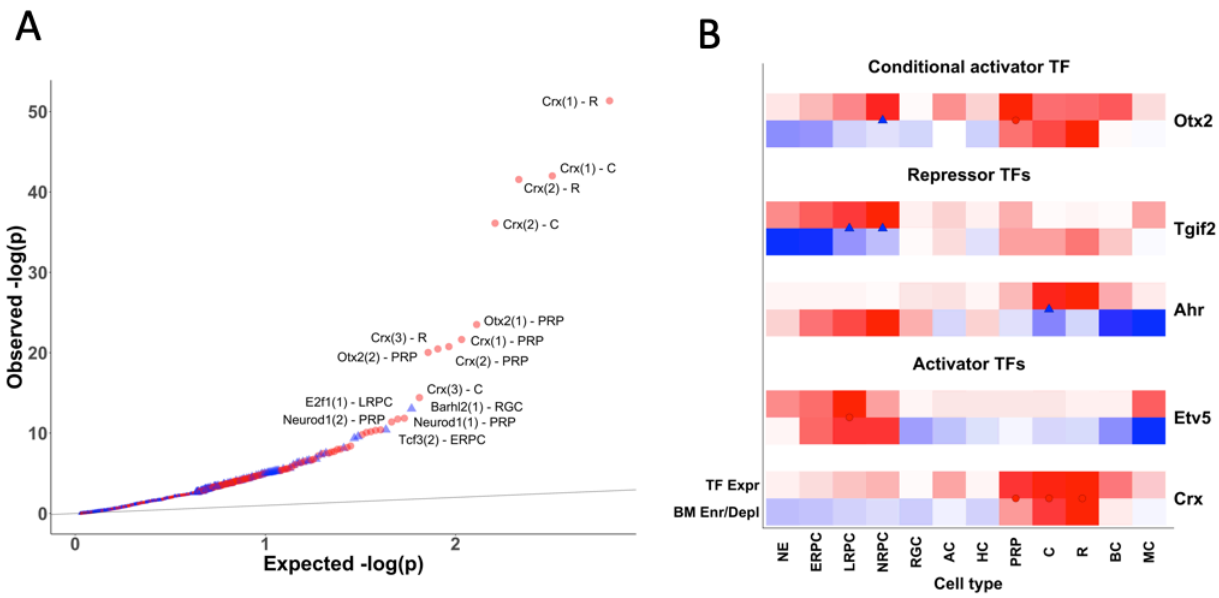

434
435

C

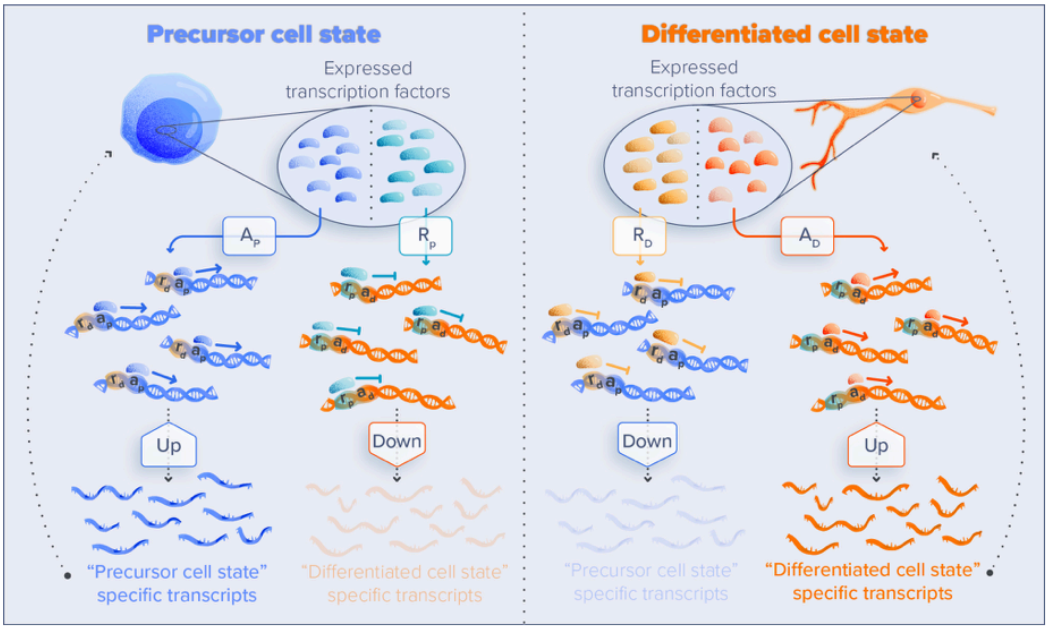
Precursor cell state
Expressed transcription factors
Differentiated cell state
Expressed transcription factors
Up
Down
Down
Up
"Precursor cell state" specific transcripts
"Differentiated cell state" specific transcripts
"Precursor cell state" specific transcripts
"Differentiated cell state" specific transcripts

D

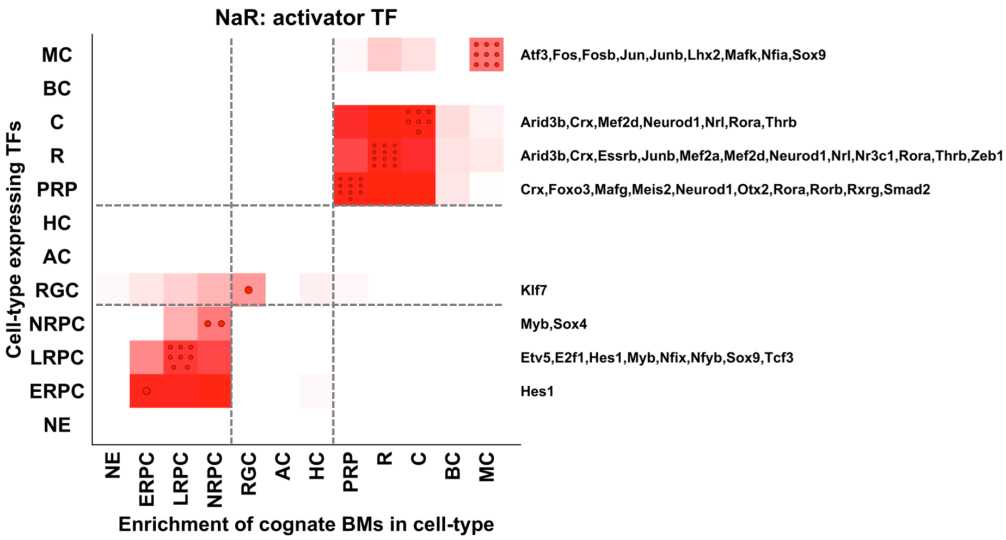
NaR: activator TF
Cell-type expressing TFs
MC
BC
C
R
PRP
HC
AC
RGC
NRPC
LRPC
ERPC
NE
Atf3,Fos,Fosb,Jun,Junb,Lhx2,Mafk,Nfia,Sox9
Arid3b,Crx,Mef2d,Neurod1,Nrl,Rora,Thrb
Arid3b,Crx,Essrb,Junb,Mef2a,Mef2d,Neurod1,Nrl,Nr3c1,Rora,Thrb,Zeb1
Crx,Foxo3,Mafg,Meis2,Neurod1,Otx2,Rora,Rorb,Rxrg,Smad2
Klf7
Myb,Sox4
Etv5,E2f1,Hes1,Myb,Nfix,Nfyb,Sox9,Tcf3
Hes1
NE ERPC LRPC NRPC RGC AC HC PRP R C BC MC
Enrichment of cognate BMs in cell-type

E

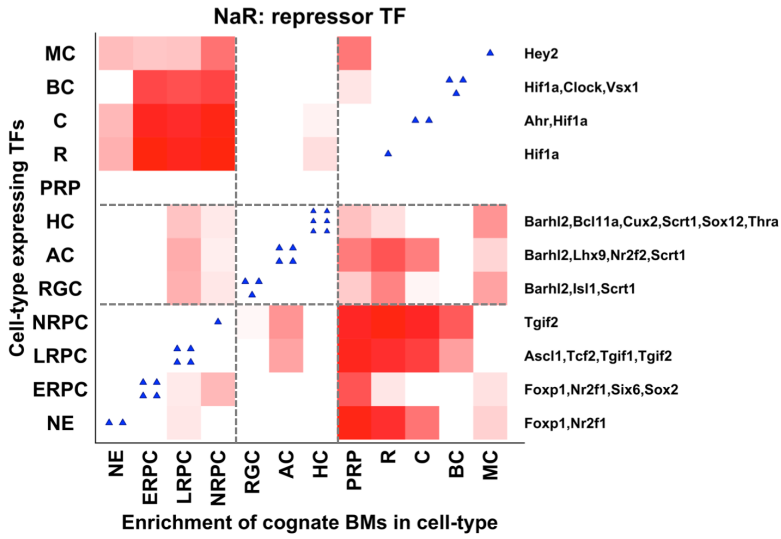
NaR: repressor TF
Cell-type expressing TFs
MC
BC
C
R
PRP
HC
AC
RGC
NRPC
LRPC
ERPC
NE
Hey2
Hif1a,Clock,Vsx1
Ahr,Hif1a
Hif1a
Barhl2,Bcl11a,Cux2,Scrt1,Sox12,Thra
Barhl2,Lhx9,Nr2f2,Scrt1
Barhl2,Isl1,Scrt1
Tgif2
Ascl1,Tcf2,Tgif1,Tgif2
Foxp1,Nr2f1,Six6,Sox2
Foxp1,Nr2f1
NE ERPC LRPC NRPC RGC AC HC PRP R C BC MC
Enrichment of cognate BMs in cell-type

Figure 5: Combined analysis of scRNA-Seq and bulk ATAC-Seq data reveals putative activator and repressor TF that may constitute regulatory toggles. (A) QQ plot of log(1/p) values of the difference in average number of binding motifs in ATAC-Seq peaks of over-expressed versus under-expressed genes for TF over-expressed in the corresponding cell type. Enrichments are indicated by red dots, depletions by blue triangles. Symbols are large for TF with q-value < 0.01, and small for TF with q-value ≥ 0.01. For the most significant effects, the name of the TF is given, as well as – between brackets - the index of the binding motif, and the cell type. The grey line corresponds to expectations assuming that all tests are true null hypotheses. **(B) Examples of activator, repressor and conditional activator TF.** Upper lines ("TF Expr", white-red color code): standardized expression pattern of corresponding TF across 12 cell types. Lower lines ("BM Enr/Depl", blue-white-red color code): standardized enrichment (red) or depletion (blue) of binding motif(s) of corresponding TF across 12 cell types. The red circles and blue triangles mark the cases that are part of (A). They require that the TF be overexpressed in the corresponding cell type, and that there is either a significant enrichment of binding motifs in overexpressed genes (red circles) or a significant depletion (blue triangles). **(C) Components of regulatory toggles and principles underlying their detection.** Shown are a hypothetical precursor (blue) and derived differentiated cell (orange). The precursor cell is expressing a number of activator (A_P, blue) and repressor TF (R_P, green). These are respectively activating and repressing target genes by binding to motifs in cis-acting regulatory elements labelled respectively as a_P and r_P. The differentiated cell is expressing its own activator (A_D, orange) and repressor TF (R_D, yellow), which are respectively activating and repressing target genes by binding to motifs in cis-acting regulatory elements labelled respectively as a_D and r_D. Genes that are overexpressed in precursor cells (under-expressed in differentiated cells) are enriched in a_P and r_D binding motifs, and depleted in a_D and r_P binding motifs. Genes that are overexpressed in differentiated cells (under-expressed in precursor cells) are enriched in a_D and r_P binding motifs, and depleted in a_P and r_D binding motifs. **(D-E) Combined enrichment profile across all cell types (X-axis) of binding motifs for all activator (upper graph) and repressor (lower graph) TF expressed in a given cell type (Y-axis) in NaR.** Standardized (across entire array) sum of signed (+ for enrichment, - for depletion) log(1/p) values for binding motifs of TF expressed in a given cell type (Y-axis). Positive values are measured by a white-red color code; values ≤ 0 are in white. For each cell type, the number of overexpressed activator TF (upper graph, red circles on diagonal) and repressor TF (lower graph, blue triangles on diagonal) are given, and their names provided on the right. The horizontal and vertical dotted lines delineate clusters I, II and III as defined in the main text.

ScATAC-Seq supports the toggle hypothesis.

To further test our toggle hypothesis, we took advantage of publicly available scATAC-Seq data for 1,792 cells isolated from retina of eight-week old mice (P56)[39]. Using 10xGenomics' Cell Ranger ATAC software we clustered the cells based on transposase accessibility of 117,073 scATAC-Seq peaks. Clusters were then assigned to specific cell-types using the same gene signatures used with the scRNA-Seq data (STable 3). Cell-specific gene expression levels were estimated as the proportion of reads mapping to ATAC-Seq peaks assigned to the corresponding gene (i.e. the transposase accessibility of the gene in that cell). Consistent with the results reported in [39], these analyses confirmed that the sample is primarily composed of R (n = 736), AC (n = 500), BC (n = 419), C (n = 91), and MC (n = 46) (Fig. 6A).

Hence, this dataset provides scATAC-Seq information for one cell type belonging to cluster II (AC) and three cell types belonging to cluster III (R, C and BC). Examining the list of activator and repressor TF reported in Fig. 5D and E, we concluded that we could use this scATAC-Seq

483 dataset to (i) test the predicted activator status of 11 of 12 TF active in C and/or R (i.e.
484 expressed in C/R and activating genes in C/R) (Arid3b, Crx, Esrrb, Junb, Mef2a, Mef2d,
485 Neurod1, Nrl, Nr3c1, Rora, Zeb1; no data available in Cell Ranger for Thrb; see Fig. 5D), and
486 (ii) test the predicted repressor status of 4 out of 4 TF active in AC (i.e. expressed in AC and
487 repressing genes in AC that are normally expressed in C/R)(Barhl2, Lhx9, Nr2f2, Scrt1; see Fig.
488 5E).
489 We first tested the 11 C/R activator TF. Cell-specific TF expression levels were estimated as
490 the proportion of reads mapping to ATAC-Seq peaks assigned to the corresponding TF-
491 encoding gene (i.e. the transposase accessibility of the TF-encoding gene in that cell). The
492 aggregate expression levels of the genes activated by the TF were estimated as the proportion
493 of reads mapping to genome-wide ATAC-Seq peaks matched to a cognate binding motif by
494 the Cell Ranger ATAC algorithm (10X Genomics)(i.e. the aggregate accessibility of the binding
495 motif of the TF of interest in that cell). Our prediction was that for C/R activator TF, both the
496 TF-encoding genes and the cognate binding motifs (genome-wide) should be transposase-
497 accessible in C and R cells (= cluster III). Visual examination of paired tSNE maps for (i) TF
498 gene accessibility and (ii) cognate TF binding motif accessibility, clearly revealed the expected
499 colocalization in C/R cells (as well as BC cells)(Fig. 6B). To more rigorously assess the statistical
500 significance of these visual impressions, we computed the correlations between the cells' TF
501 gene accessibility and TF binding motif accessibility. The correlation was positive for 11/11
502 C/R activators ($p_{Spearman} \leq 0.05$ for 9/11)(Fig. 6C and SFig. 9).
503 We then performed the same analyses for the four AC repressor TF. Visual examination of
504 the paired tSNE plots revealed a striking contrast with the 11 activator TF: repressor TF gene
505 accessibility was highest in AC (cluster II), while repressor TF binding motif accessibility was
506 highest in the other cell types (cluster III) (Fig. 6B). Accordingly, the correlation between the
507 cells' TF gene accessibility and TF binding motif accessibility was negative for the four AC
508 repressors ($p_{Spearman} \leq 0.05$ for 4/4)(Fig. 6C and SFig. 9). The probability to observe a
509 positive correlation for 11/11 predicted activator TF and a negative correlation for 4/4
510 predicted repressor by chance alone is $3x10^{-5}$.
511

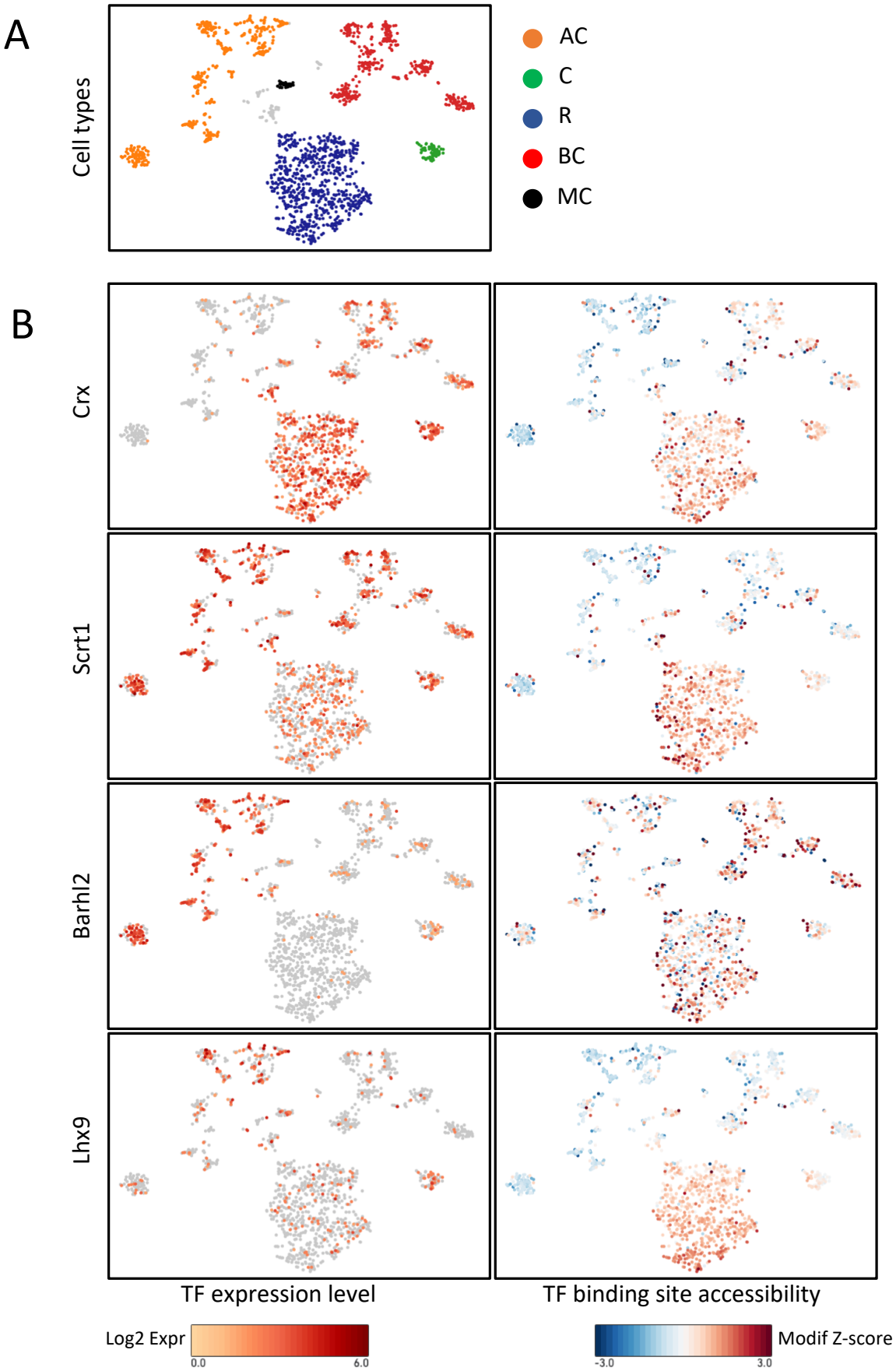
A
Cell types
AC
C
R
BC
MC
B
Crx
Scrt1
Barhl2
Lhx9
TF expression level
TF binding site accessibility
Log2 Expr
0.0
6.0
Modif Z-score
-3.0
3.0

512

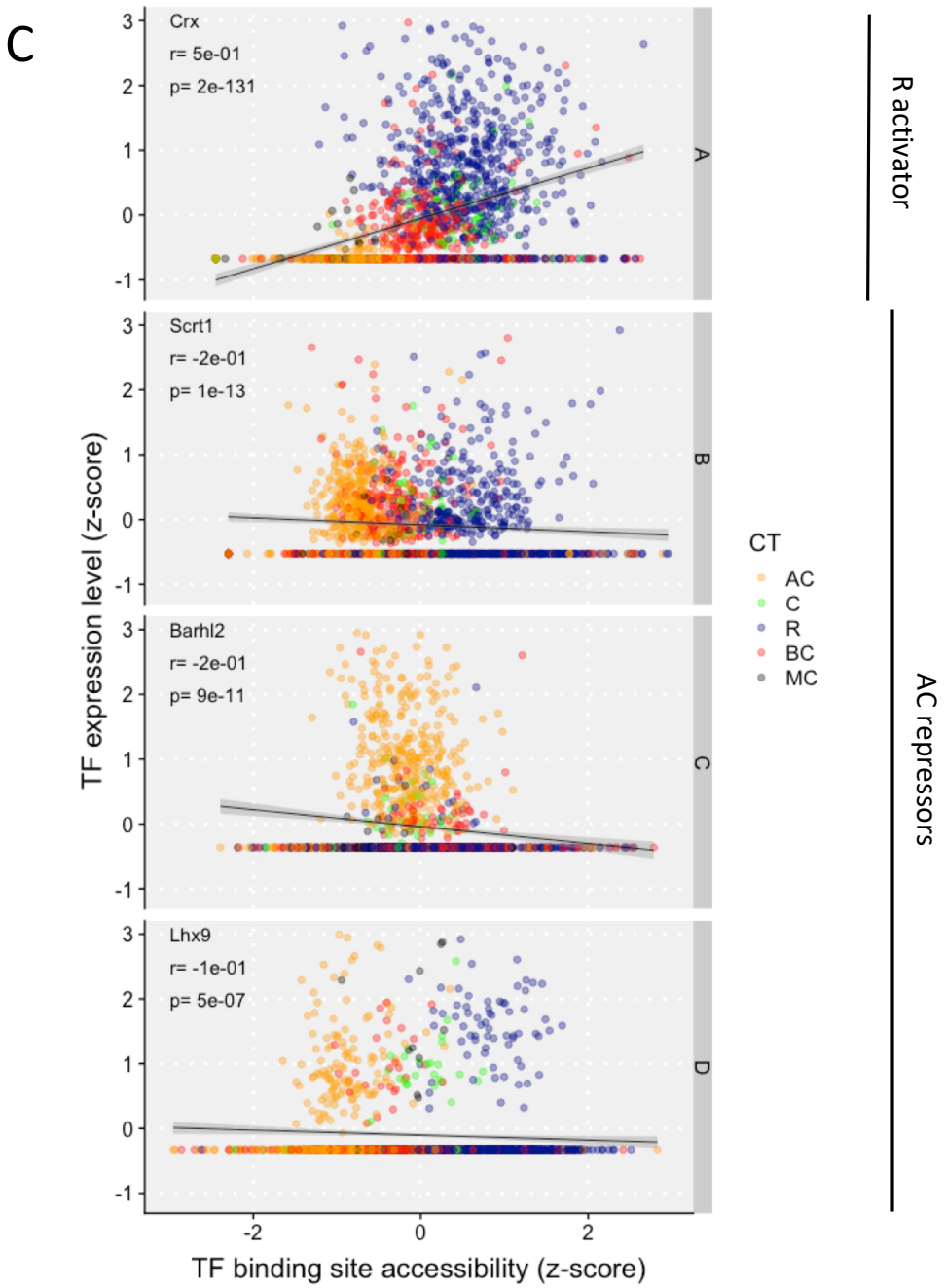

Figure 6: Single-cell ATAC-Seq data support the regulatory toggle model. (A) scATAC-Seq based tSNE plot constructed with the Cell Ranger ATAC software (10xGenomics) and the data from Norrie et al. [38]. Cells were assigned to cell-types based on the accessibility of the marker genes reported in STable 3. Cell-type abbreviations and colors are as in the previous figures. The number of cells per cell type are in good agreement with [39]. **(B)** (Left panels) Expression levels of one C/R activator (Crx) and three presumed AC repressors (Scrt1, Barhl2, Lhx9) inferred from their transposase accessibility, showing higher accessibility of Crx in R, C and BC, and higher accessibility of Scrt1, Barhl2 and Lhx9 in AC. (Right panels) Aggregate genome-wide transposase accessibility of cognate binding motifs, showing higher accessibility of Crx motifs in R, C and BC (i.e. same as for Crx itself), and higher accessibility of Scrt1, Barhl2 and Lhx9 motifs in R, C (and BC) than in AC (i.e. opposite as for corresponding TF). **(C)** Scatter plots showing the correlation between gene-specific TF transposase accessibility (y axis) and corresponding genome-wide TF binding motif transposase accessibility (x axis). Dots correspond to individual cells. All correlations are highly significant, positive for the C/R activator, and negative for the AC repressors. See SFig. 9 for plots of 11 C/R activators and 4 AC repressors.

526 ***Comparing the effects of activator and repressor TF between NaR and 3D-RA using scRNA-***
527 ***Seq and bulk ATAC-Seq data.***
528 We repeated the same analyses as described above for the 13 major cell types detected in
529 3D-RA (including RPE). We identified 18 activator TF, 24 repressor TF, 3 conditional activator
530 TF, and 2 dual TF (STable 12&14). Thirty-eight of these 47 TF overlapped with those found in
531 NaR. Analyzing the combined effect of TF overexpressed in a given cell type largely confirmed
532 the three clusters detected in NaR. RPE appear to be part of cluster (I), while 3D-RA MC could
533 not be classified as no over-expressed TF (whether activator or repressor) could be detected
534 in this cell type in 3D-RA (Fig. 8A&B). The degree of enrichment/depletion of TF binding
535 motifs (measured by the signed (+ for enrichment, - for depletion) log(1/p)) in the different
536 cell types was highly correlated between NaR and 3D-RA ($r= 0.82$, $p < 2.2e-16$)(Fig. 8C). The
537 slope of the regression line was significantly < 1 suggesting that, overall, the TF's activator
538 and repressor effects might be slightly reduced in 3D-RA when compared to NaR.
539 Alternatively, statistical power could be slightly higher in NaR due to the larger number of
540 analyzed cells. Outliers included Crx and Otx2 which appeared to have more pronounced
541 activator effects in PRP of 3D-RA than of NaR (Fig. 8C&D). This may be related to the fact that
542 the 3D-RA culture conditions were designed to "push" PRP development (see also Fig. 2J).
543 Other outliers were Etv1, Etv5, Hes1 and Zbtb7a which pointed towards TF-driven differences
544 in the NaR and 3D-RA transcriptomes of HC and MC (Fig. 8C). Binding motifs for this group of
545 TF were enriched in genes that were under-expressed in MC of NaR but this was not observed
546 in 3D-RA (dots near horizontal dotted line Fig. 8C), while being enriched in genes that were
547 under-expressed in HC of 3D-RA but this was not observed NaR (dots near vertical dotted line
548 in Fig. 8C)(Fig. 8D). Of note, binding motifs of Etv1, Etv5, Zbtb7a, but not Hes1 are partially
549 overlapping (SFig. 10). The prediction is therefore that (i) there are genes that are under-
550 expressed in MC of NaR but not in MC of 3D-RA and whose ATAC-Seq peaks have a high
551 density in Etv1/Etv5/Hes1/Zbtb7a binding motif, and (ii) there are genes that are under-
552 expressed in HC of 3D-RA but not in HC of NaR and whose ATAC-Seq peaks have a high density
553 in Etv1/Etv5,Hes1/Zbtb7a binding motif. Indeed, we found that there was a very strong
554 coincidence between the density of Etv1/Etv5/Hes1/Zbtb7a binding motifs and the two
555 predicted expression patterns (under-expressed in MC of NaR but not of 3D-RA; under-
556 expressed in HC of 3D-RA but not of Nar)(Fig. 8E&F). We identified 77 genes under-expressed
557 in MC of NaR but not of 3D-RA with high density in Etv1/Etv5/Hes1/Zbtb7a bindings motifs,

558 and 61 genes under-expressed in HC of 3D-RA but not of Nar with high density in
559 Etv1/Etv5/Hes1/Zbtb7a bindings motifs (STable 15). We submitted these gene lists to
560 Reactome. The pathways that were enriched overlapped strongly between the two lists
561 (although only eight genes were common to both lists) and pertained mainly to RNA stability
562 and translation and to a lesser extent to the cell cycle (STable 15). They coincided remarkably
563 well with the Reactome pathways that were highlighted by the genes that appeared in the
564 scRNA-Seq analyses to be more strongly expressed in MC of 3D-RA than of NaR (found entities
565 labelled in orange [3D-RA > NaR, column MC] in Fig. 3B). Thus, the combined scRNA-Seq and
566 ATAC-Seq analysis reveals that part of the difference between MC of Nar and 3D-RA is due to
567 perturbed expression of genes that are controlled by the Etv1/Etv5/Hes1/Zbtb7A TF
568 squadron. Of note, these effects appeared largely independent of differences in the
569 expression levels of the corresponding TF (in MC/HC) between NaR and 3D-RA per se: Etv1
570 was the only TF to have a significantly higher expression level in 3D-RA than NaR in MC (STable
571 7).

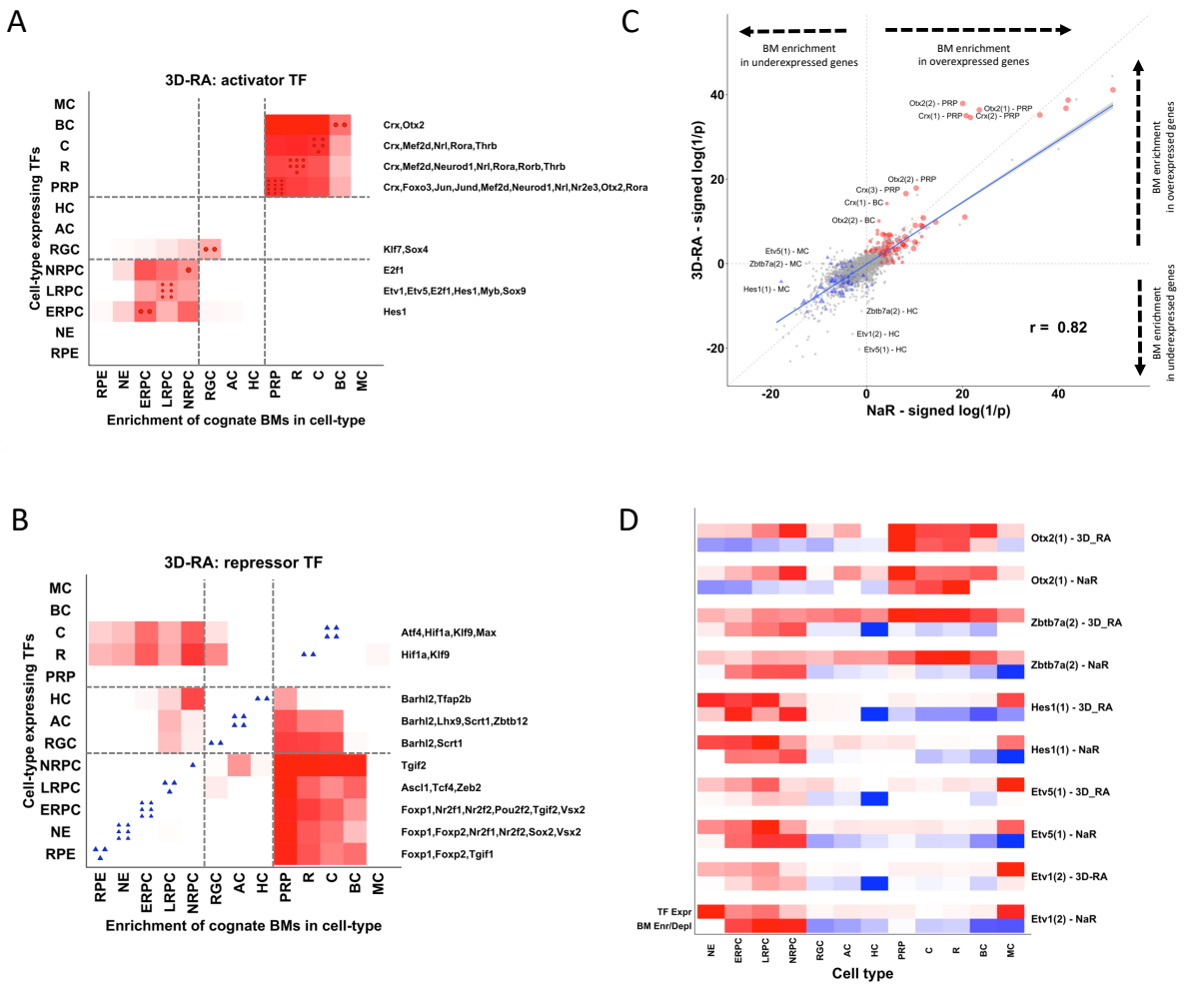

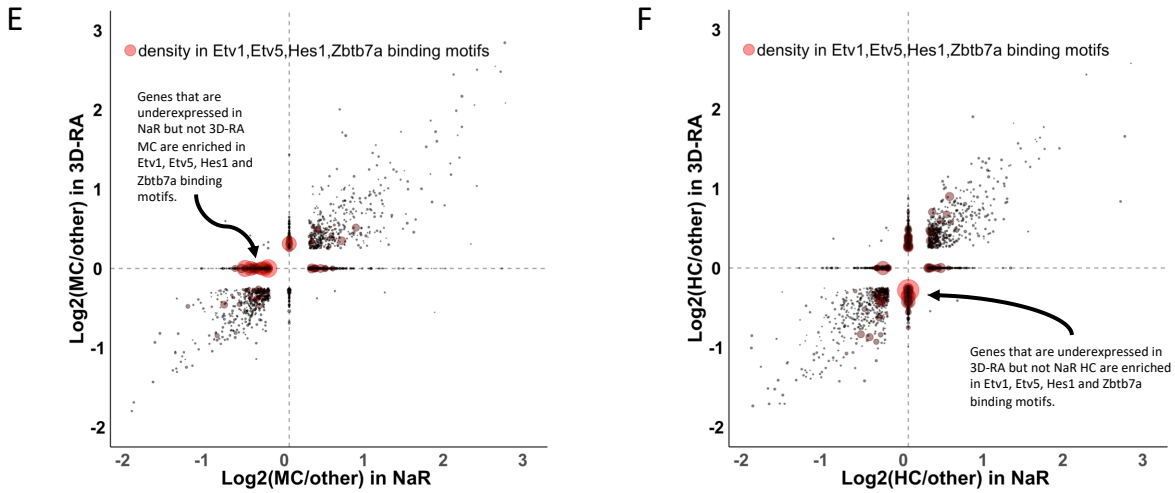

Figure 8: Comparing the operation of regulatory toggles between Nar and 3D-RA. (A,B) Combined enrichment profile across all cell types (X-axis) of binding motifs for all activator (A) and repressor (B) TF expressed in a given cell type (Y-axis) in 3D-RA. Standardized (across entire array) sum of signed (+ for enrichment, - for depletion) log(1/p) values for binding motifs of TF expressed in a given cell type (Y-axis). Positive values are measured by a white-red color code; values ≤ 0 are in white. For each cell type the number of overexpressed activator TF (upper graph, red circles on diagonal) and repressor TF (lower graph, blue triangles on diagonal) are given, and their names provided on the right. The horizontal and vertical dotted lines delineate clusters I, II and III as defined in the main text. **(C) Comparison of the log(1/p) values for enrichment (+)/depletion (-) of TF binding motifs across cell types between NaR (X-axis) and 3D-RA (Y-axis).** Red circles: values for activator TF in the cell type in which they are overexpressed. Blue triangles: values for repressor TF in the cell type in which they are overexpressed. Small grey circles: values for cell types in which the corresponding TF is not overexpressed. The identity of outlier TF is given, as well as – between brackets - the index of the binding motif, and the cell type. "r" = correlation coefficient. **(D)** Expression levels (red scale) (upper line) and enrichment (red scale)/depletion (blue scale) of binding motifs in overexpressed genes (lower line) in NaR and 3D-RA for five TF highlighted in Fig. 8C. **(E)** Log2 fold over (+) or under (-) expression of genes in MC relative to the other cell types in NaR (x-axis) and 3D-RA (y-axis). When the fold-change in expression is not significantly different from 0, the gene receives 0 value in the corresponding sample type (i.e. on the horizontal line for 3D-RA, and on the vertical line for NaR). The size and redness of the symbols measures the density in the weighted sum of the binding motifs for Etv1, Etv5, Hes1 and Zbtb7a for the corresponding gene. One can clearly see that the genes that are significantly underexpressed in NaR but not in 3D-RA (genes on left side of horizontal line) are enriched in genes with high density of TF binding motifs. **(F)** As (E) for HC. One can clearly see that the genes that are significantly underexpressed in 3D-RA but not in NaR (genes on bottom side of vertical line) are enriched in genes with high density of TF binding motifs.

Discussion

We herein use scRNA-seq to compare the unfolding of the epigenetic program in *in vivo* versus *in vitro* (from iPS cells) derived murine retina at four matched development stages encompassing the presumed emergence times of the major retinal cell types (E13 vs DD13, P0 vs DD21, P5 vs DD25 and P9 vs DD29). Results obtained by combining information from (i) the analysis of four developmental stages, (ii) 3D UMAP manifolds visualized in virtual reality (http://www.sig.hec.ulg.ac.be/giga), and (iii) RNA velocity analysis, are in good agreement with the previously reported, main retinal developmental trajectories (Fig. 1F). We identify

606 >4,000 genes that are differentially expressed during *in vivo* retinal differentiation
607 corresponding to tens of biological pathways pertaining to the cell cycle, gene expression,
608 signal transduction, metabolism, cell biology and development (Fig. 3). Several of these
609 pathways were previously highlighted when submitting differentially expressed genes
610 identified from the analyses of bulk RNA-Seq data from multiple time points (E11 to P28)
611 during retinal development [40]. Our data now allows to assign highlighted pathways to
612 individual cell types. Differentially expressed genes include ~300 TF, of which ~100 are at
613 least 1.5 times more strongly expressed in one specific retinal cell type when compared to all
614 other ones. The latter include 19 TF not yet described in the field of retinal development
615 which could serve as a starting point for functional investigations of the roles of these TF in
616 retinogenesis and physiology.
617 We generated bulk ATAC-Seq data for three of the four analyzed developmental stages in
618 both NaR and 3D-RA. This allowed us to identify 98,181 putative regulatory elements assigned
619 (by proximity) to 19,171 genes, that are accessible during retinal development. This collection
620 of ATAC-Seq peaks also allowed us to test the activity of 151 TF shown by scRNA-Seq to be
621 differentially expressed during retinal development, and which have known binding motif(s).
622 For 31 of these (considering both NaR and 3D-RA; STable 12), we observed an enrichment (q-
623 value < 0.01) of binding motifs in ATAC-Seq peaks of genes that are over-expressed in the
624 same cell type as the TF. This is what is expected for TF that act predominantly as activators
625 in the corresponding cell type. Reassuringly, the list of predicted activators includes several
626 TF that are known to play key roles during retinal development such as Crx, Neurod1, Nr2e3,
627 Nrl, Rora, Rorb, Rxrg, Sox9 and Thrb [30, 41-43].
628 Unexpectedly, for 31 other TF we observed a significant depletion of binding motifs in the
629 ATAC-Seq peaks of genes that were over-expressed in the same cell type as the TF. This is
630 what is expected if the TF acts predominantly as a repressor in that cell type. Accordingly, the
631 list comprises several acknowledged repressors including Atf4 [44], Barhl2 [45,46], Bcl11a
632 [47], Foxp1 [48,49], Foxp2 [50], Hey2 [51,52], Scrt1 (= Scratch Family Transcriptional
633 Repressor 1) [53], Six6 [54], Sox2 [55], Tgif1 [56], Tgif2 [56], Vsx1 [57], Vsx2 [58], Zeb2 [59],
634 and Zbtb12 [60]. Of interest, the list of putative repressors comprises three TF that have been
635 labelled as "pioneer factors" (i.e. TF that engage with closed chromatin to open it and make
636 it subsequently accessible to other TF [61]), including Ascl1 [62,63], Sox2 [62], and Isl1 [64].
637 If the pioneer factor were transiently expressed in retinal progenitor cells (as observed for

638 Ascl1 and Sox2, but not Isl1; STable 12), rendering chromatin accessible to activator TF that
639 are expressed and operate in later stages of development, this may conceivably also generate
640 the observed depletion of binding motifs in the ATAC-Seq peaks of genes that are over-
641 expressed in the same cell type as the pioneer TF. We note that three of the TF in the list of
642 putative repressors (Ahr, Hif1α and Clock), which are typically regarded as paradigmatic
643 activators, are functionally connected: Ahr competes with Hif1α for binding to the nuclear
644 translocator protein Arnt and – possibly - with Clock for binding to Arnt-similar Bmal1 [65]. It
645 is tempting to speculate that this connection may underpin the fact that these three
646 supposedly activator TF appear as repressors in our analyses.
647 For 10 TF (Etv1, Fosb, Hes1, Jun, Junb, Lhx2, Otx2, Pax6, Sox11 and Tcf3, STable 12),
648 overexpression of the TF was accompanied by binding motif enrichment in some cell type(s),
649 and depletion in other(s). We labelled these as "conditional activator" TF, meaning that the
650 presence of the TF is necessary but not sufficient to exert its effect on transcription. This
651 could for instance reflect the need for post-translational modification of the TF [66], or for
652 cooperation with other TF or cofactors [67], or the fact that the target sites of the TF are not
653 yet accessible requiring further chromatin remodeling [39].
654 It is increasingly recognized that many TF act both as activator or repressor in different or
655 even in the same cell type, depending (i) on the combination of TF that bind to a given cis-
656 acting regulatory element, as well as (ii) the coregulators (devoid of own DNA binding domain)
657 that they recruit to the regulatory element [67,68]. Accordingly, for many of the TF listed in
658 STable 12, both activator and repressor effects have been reported in the literature. The
659 approach that we have used (i.e. searching for an enrichment or a depletion of binding motifs
660 for an overexpressed TF in the ATAC Seq peaks of all other overexpressed genes) reveals the
661 activity of the TF (activation vs repression) that predominates in a given cell type. For the 31
662 TF whose predominant activity was of the repressor type, we could nearly always identify one
663 or more cell types in which the ATAC-Seq peaks of over-expressed genes were enriched in the
664 corresponding binding motif (despite the fact that the TF was not over-expressed in that cell
665 type). This strongly suggests that the corresponding repressor specifically targets genes that
666 define another retinal cell type. We revealed a clear relationship between the cell type(s) in
667 which the repressor TF is expressed and the cell type(s) in which its target genes are
668 expressed, allowing us to define three clusters: (I) NE, ERPC, LRPC and NRPC, (II) RGC, AC and
669 HC, and (III) PRP, C, R, BC and MC (Fig. 5D&E). Repressors TF expressed in cluster I (precursor

670 cells) primarily target genes defining cell types of cluster III (primarily photoreceptor and
671 bipolar cells), repressor TF expressed in cluster III primarily target genes defining cell types of
672 cluster I, and repressor TF expressed in cluster II target genes defining cell types of both
673 clusters I and III. Based on these findings, we propose that combinations of activator and
674 repressor TF constitute regulatory toggles that help ensure cell type-specific gene expression
675 and hence cellular identity (Fig. 5C). Our results suggest that the hypothesized regulatory
676 toggles involve multiple activators and repressors. This may confer robustness to the system,
677 and enable differentiation of multiple cell types. It also indicates that perturbing TF one at a
678 time, whether by overexpression or knock-out/down, may not be effective to dissect such
679 multifactorial toggles. It may be necessary to perform pooled screens using CRISPR libraries
680 targeting several candidates at once (at high multiplicity of infection) in Perturb-Seq like
681 experiments conducted in 3D-RA [69] in order to induce detectable alterations in cellular
682 behavior.
683 We took advantage of publicly available scATAC-Seq data of adult (P56) retina of the mouse
684 (providing information about cell type clusters II and III) [39] that allowed us to test two
685 components of our regulatory toggle hypothesis in an independent data set interrogated with
686 a distinct technology: the effect of 11 TF predicted to operate as activators in cluster III, and
687 the effect of 4 TF predicted to operate as repressors in cluster II. Our analyses provide a vivid
688 visual illustration of (i) the coincident (i.e. in the same cell type) expression of activator TF and
689 their target genes (measured by increased transposase accessibility of both TF-encoding gene
690 and genome-wide ATAC-Seq peaks encompassing the cognate binding motif, respectively),
691 and (ii) the discrepant (i.e. in distinct cell types) expression of repressor TF and their target
692 genes measured in the same manner. Visual impressions were substantiated by highly
693 significant positive (activator TF) and negative (repressor TF) correlations between the
694 transposase accessibility of the TF-gene and the transposase accessibility of ATAC-Seq peaks
695 encompassing the cognate binding-motifs (Fig. 6 and SFig. 9). While the marked contrasting
696 behavior of predicted activator and repressor TF in this assay supports the pertinence of our
697 model, its biological interpretation is not trivial. It is easy to understand that if an activator
698 TF is expressed in a given cell (as testified by the openness of the chromatin surrounding it)
699 and if it is active in that cell, regulatory elements to which it binds (by recognizing cognate
700 motifs in it) to activate target genes will be open and hence accessible as well. But what
701 about the opposite pattern observed for candidate repressor TF? The fact that ATAC-Seq

702 peaks encompassing binding motifs for a repressor are primarily closed in the cell type in
703 which the repressor is expressed suggests that the repressor TF is largely effective and that it
704 contributes to closing the regulatory elements to which it has or is bound. The fact that these
705 same peaks are open in cell types in which the repressor is not expressed suggests that the
706 corresponding regulatory elements encompass binding motifs for both activator and
707 repressor TF. This prediction is substantiated by the observation of strong positive
708 correlations between the density of binding motifs (number of binding motifs divided by peak
709 size) for repressor and activator TF in the utilized scATAC-Seq data (SFig. 11). Thus, our data
710 suggest that the same regulatory elements are used to activate gene expression in the cell
711 type(s) where the gene product is needed, as well as to repress gene expression in the cell
712 type(s) in which expression of the gene is unwanted.
713
714 We show that 3D-RA broadly recapitulate the in vivo developmental program and
715 trajectories. However, developmental trajectories appear less canalized in 3D-RA when
716 compared to NaR, PRP to develop earlier and at the expense of other cell types, and terminal
717 differentiation of BC to be incomplete (Fig. 2). We identify ~3,000 genes that are differentially
718 expressed between 3D-RA and NaR in at least one cell type, and identify the corresponding
719 biological pathways pertaining in particular to the rate of cell division which is reduced in 3D-
720 RA RPCs when compared to NaR, post-transcriptional and translational mechanisms which
721 appear exacerbated in the majority of 3D-RA cell type when compared to NaR, signal
722 transduction via WNT and Notch pathways which are diminished in 3D-RA RPCs when
723 compared to NaR, 3D-RA differentiated cells which appear less functional with less
724 phototransduction cascade activity and decrease synapse formation, and finally apoptosis
725 and stress response which are increased at the latest stages of 3D-RA culture. As for NaR,
726 several of these perturbed pathways were highlighted before in analyses of bulk scRNA-Seq
727 data obtained during the development of NaR and 3D-RA [40], and can now be assigned to
728 cell type-specific transcriptome perturbations. Strikingly, the perturbed pathways show a
729 highly significant overlap with those that were shown to be differentially expressed during
730 the in vivo development of NaR. We show that TF that are differentially expressed during in
731 vivo retinal development are particularly sensitive to the iPSC culture conditions. This is likely
732 to drive the perturbations of the above-mentioned biological pathways.

733 We show how scRNA-Seq and bulk ATAC-Seq can be combined to gain novel insights into what
734 may underpin differences observed between the NaR and 3D-RA transcriptomes. As an
735 example, the comparison between MC from NaR and 3D-RA revealed 418 genes that were
736 more strongly expressed in NaR when compared to 3D-RA (NaR > 3D-RA), and 424 that were
737 more strongly expressed in 3D-RA (3D-RA > NaR) (STable 7). The first list of genes (NaR > 3D-
738 RA) was not enriched for any Reactome pathway, but the second (3D-RA > NaR) highlighted
739 53 of these (STable 8), corresponding to five subsets of "found entities" (five colors in MC
740 column (3D-RA > NaR) in Fig. 3B). One of these subsets (orange set, rich in genes encoding
741 ribosomal proteins) highlighted pathways related to RNA stability (NMD), RNA translation,
742 selenocystein metabolism and signaling by ROBO receptors. Combined scRNA-Seq and ATAC-
743 Seq data indicated that genes with high density of binding motifs for Etv1, Etv5, Hes1 and
744 Zbtb7a in their ATAC-Seq peaks are underexpressed in MC of NaR relative to 3D-RA (Fig.
745 8E&F). These four TF are expressed at relatively high and comparable levels in both NaR and
746 3D-RA. We identified the corresponding genes and subjected them to Reactome analysis.
747 They identified – to a large extent – the same pathways as the orange gene subset defined
748 above. Thus, the differences between NaR and 3D-RA MC with regards to the corresponding
749 pathways are most likely driven by perturbations of the Etv1, Etv5, Hes1 and Zbtb7a group of
750 TF. Examination of their transcriptional and binding motif enrichment/depletion profile
751 across cell types (Fig. 8D) suggests that Etv1, Etv5 and Hes1 operate as "conditional TF" (as
752 defined above) in NaR: despite still being present in MC they do not have the activator effect
753 in these cells as seen in retinal progenitor cells (hence the observed depletion in the NaR MC
754 transcriptome). In 3D-RA MC, they may still have "residual" activator activity which would
755 explain why the depletion is not seen. Zbtb7a is clearly distinct from the other three: it is
756 most strongly expressed in PRP, C and R, yet its binding motifs are primarily found in genes
757 expressed in retinal progenitor cells. How and why genes enriched in Zbtb7a motifs would
758 be underexpressed in NaR but not 3D-RA MC remains unclear. Yet these examples show how
759 studying the regulatory toggle landscape may become a valuable approach to monitor how
760 closely organoids recapitulate native development.
761

762 **Materials and methods**

763 ***Generation of iPSC-derived retinal aggregates.*** *Maintenance of iPSCs:* The mouse iPSC-
764 NrlGFP line was obtained from the laboratory of Retinal Regeneration from the RIKEN Center

765 for Developmental Bioloy (CDB) (Kobe, Japan). These iPSCs were generated from fibroblasts
766 [70] of C57BL/6 Nrl-eGFP transgenic mice [20]. iPSCs were maintained according to [71] in
767 60-mm Petri dishes (0,6 x 10^5 cells total per dish) coated with 0.1% gelatin (G2625, Merck,
768 Darmastadt, Germany) in Glasgow's Minimum Essential Medium (GMEM, 11710035,Thermo
769 Fisher Scientific, Waltham, MA) supplemented with 10% Fetal Bovine Serum (FBS, #04-001-1,
770 Biological Industries, Beit HaEmek, Israel), 1 mM sodium pyruvate (Merck), 0.1 mM MEM
771 Non-Essential Amino Acids Solution (NEAA, Thermo Fisher Scientific), 0.1 mM 2-
772 mercaptoethanol (2-ME, Wako Pure Chemical, Osaka, Japan), 100 U/mL penicillin-
773 streptomycin (Thermo Fisher Scientific), 1000 U/mL of Leukemia inhibitory factor (Esgro LIF,
774 Merck), 3 µM CHIR99021 (BioVision, Milpitas, CA) and 1 µM PD0325901 (Stemgent,
775 Cambridge, MA). *Generation of iPSC-derived retinal aggregates :* Differentiation of iPSCs into
776 retinal aggregates was done using the SFEBq (serum-free floating culture of embryoid body-
777 like aggregates with quick re-aggregation) method according to [21] with some modifications
778 following [71] and [72]. The iPSCs were dissociated (DD0) after 4-5 days of maintenance using
779 0.25% trypsin / 1 mM EDTA (Thermo Fisher Scientific) at 37°C for 2 minutes. Embryoid body-
780 like aggregates were formed by adding 5,000 cells/dish in a low binding 96-well microplate
781 (174925, Nunclon Sphera, Thermo Fisher Scientific) in 100 µL of differentiating medium. The
782 differentiating medium is composed of GMEM (Thermo Fisher Scientific), 0.1 mM AGN193109
783 (Toronto Research Chemicals, Toronto, Canada), 5% of Knock-out Serum Replacement (KSR,
784 Thermo Fisher Scientific), 1 mM Sodium Pyruvate (Merck), 0.1 mM NEAA (Thermo Fisher
785 Scientific) and 0.1 mM 2-ME (Wako). At DD1, 20 µL of Matrigel Growth Factor Reduced
786 Basement Matrix (Corning, Corning, NY) was added to obtain a final concentration equal to
787 2%. The cells were left in this medium untill DD8. At DD8, retinal aggregates were picked up
788 and transferred in 60-mm Petri dishes in maturation medium composed of Dulbecco's
789 Modified Eagle's Medium (DMEM)/F-12 with glutamax (Thermo Fisher Scientific), 1% of N-2
790 supplement (Thermo Fisher Scientific) and 100 U/mL penicillin-streptomycin (Thermo Fisher
791 Scientific). 0.5 µM retinoic acid (DD13 to DD18) (#R2625, Merck), 1 mM of L-taurine (DD13
792 to DD29) (#T8691,Merck) and 1% FBS (DD21 to DD29) (Biological Industries) were added to
793 this maturation medium. Taurine and retinoic acid promote rod photoreceptors
794 differentiation [73]. From DD8 to DD29 cultures were maintained in hyperoxic conditions
795 (37°C, 40% O_2 / 5% CO_2). Development of retinal aggregates was monitored and GFP

796 expression was confirmed from DD18 using an EVOS FL digital inverted fluorescence
797 microscope (Thermo Fisher Scientific).
798 ***Immunofluorescence.*** Retinal aggregates were fixed for 20 minutes at room temperature in
799 4% paraformaldehyde (PFA) in phosphate saline (PBS) at pH 7.4. They were equilibrated
800 overnight in 30% sucrose (in PBS) at 4°C before cryoprotection. Eyeballs from wild type
801 C57BL/6 mice, used as positive controls, were enucleated and punctured in the center of the
802 cornea before fixation for 1 hour in 4% PFA and at room temperature, then washed in PBS
803 and incubated in sucrose 30% at 4°C overnight. Samples were embedded in Richard-Allan
804 Scientific NEG-50 Frozen Section medium (Thermo Fisher Scientific). Slices of 10 to 15 µm
805 were generated with a cryostat and placed on Superfrost Ultra Plus slides (Thermo Fisher
806 Scientific). For immunofluorescence, slides were first incubated in Blocking One solution
807 (Nacalai Tesque, Kyoto, Japan) for 1 hour at room temperature, then at 4°C overnight with
808 primary antibodies diluted in Dako REAL Antibody Diluent (Agilent, Santa Clara, CA). We used
809 the following primary antibodies: rabbit antibody against Protein Kinase Cα diluted at 1:500
810 (Antibody Registry ID: AB_477345, Merck), rabbit antibody against Recoverin at 1:1000
811 (AB_2253622, Merck), rabbit antibody against Calretinin at 1:500 (AB_2313763, Swant,
812 Marly, Switzerland), rabbit antibody against Pax6 at 1:100 (AB_2313780, BioLegend, San
813 Diego, CA), mouse antibody against RET-P1 at 1:1000 (anti-Rhodopsin, AB_260838, Merck),
814 sheep antibody against Chx10 at 1:1000 (AB_2314191, Exalpha Biologicals, Shirley, MA). After
815 24 hours, slides were washed three times for 5 minutes in 0.05% PBS- Tween then incubated
816 with appropriate secondary antibodies in the dark at room temperature (anti-IgG rabbit A488
817 and A647, anti-IgG mouse A555 and anti-IgG sheep A555, all from Thermo Fisher Scientific)
818 and 1:1000 4',6-diamidino-2-phenylindole (DAPI) in Dako REAL Antibody Diluent. After
819 another wash in PBS-Tween, slides were mounted with FluorSave Reagent (Merck). Images
820 were taken with a Nikon Eclipse T_i confocal microscope.
821 ***Single cell RNA Seq.*** *Dissociation of native retinal tissue and 3D-culture retinal aggregates:*
822 The dissociation of mouse retinas and 3D retinal aggregates was inspired by the protocol of
823 Macosko et al. [74]. Eyeballs of C57BL/6 wild type mice were enucleated at time points E13,
824 P0, P5 and P9. Dissected retinas were placed in Dulbecco's Phosphate Buffered Saline (DPBS,
825 Thermo Fisher Scientific). Optic vesicule (OV)-like structures of the iPSCs derived 3D retinal
826 aggregates were cut at DD13, DD21, DD25 and DD29 and transferred in DPBS as well. Papain
827 4 U/mL (Worthington Biochemical Corporation) was added to the samples. The solution

828 containing the retinas and the OV-like structures was maintained at 37°C for 45 and 30
829 minutes, respectively. 0.15% ovomucoid (Worthington Biochemical Corporation, Lakewood,
830 NJ) was added for papain inhibition. Samples were centrifuged in order to eliminate the
831 supernatant and cells were resuspended in DPBS. Cell numbers and proportion of living cells
832 were estimated by Trypan Blue staining and using a Countess II cell counter (Thermo Fisher).
833 *scRNA-Seq:* We generated two biological replicates for stages 1 to 3 (NaR and 3D-RA) and one
834 biological replicate for stage 4 (NaR and 3D-RA). We loaded ~15,700 cells for biological
835 replicate 1 (stage 1-4) and ~10,000 cells for biological replicate 2 (stage 1-3) in a Chromium
836 Controller instrument (10X Genomics, Pleasanton, CA). Sequencing libraries were generated
837 using Chromium Single Cell 3' reagent kits v2.0 following the recommendations of the
838 manufacturer (10X Genomics). Actual sequencing was conducted on an Illumina NextSeq 500
839 instrument (Illumina, Sand Diego, CA). *Bioinformatic analyses:* Demultiplexing, alignment,
840 filtering, barcode counting, UMI counting, and aggregation of multiple runs were conducted
841 using Cell Ranger v2.1.1 (10X Genomics). Further filtering, k-means clustering, UMAP
842 projection were conducted using the Seurat software suite
843 (https://satijalab.org/seurat/)[23]. Velocity analysis was performed using the Velocyto R [11]
844 and scvelo [12] packages. Single- cell trajectory inference and pseudotime analyses were
845 conducted using Monocle2 (http://cole-trapnell-lab.github.io/monocle-release/)[14].
846 ***ATAC-Seq.*** *Data generation:* ATAC-seq libraries were constructed on NaR (E13, P0, P5) and
847 3D-RA (DD13, DD21, DD25) samples with biological replicates following the Omni ATAC
848 protocol [36]. We used 50,000 cells per reaction taken from the cell suspensions prepared for
849 the scRNA-seq. We tested two different amounts of Tagment DNA TDE1 enzyme (1 and 2 µl
850 in a 50 µl reaction volume) (Illumina) per sample. Genomic DNA (gDNA) libraries were also
851 prepared using 50 ng of gDNA isolated from NaR P5 and 3D-RA DD25 cells by following the
852 Nextera DNA Sample Preparation Guide (Illumina). The libraries were purified using the
853 MinElute PCR purification kit (Qiagen, Venlo, Netherlands) followed by 13 and 5 cycles of PCR-
854 amplifications for ATAC-seq and gDNA libraries, respectively. After validating library size
855 distribution using the QIAxcel capillary electrophoresis (Qiagen), the libraries were further
856 purified using the SPRIselect reagent to remove large DNA molecules (a right-side size
857 selection with 0.55X followed by 1.5X ratios of beads) (Beckman Coulter, Brea, California). On
858 average 10.6 millions of 38-nucleotide paired-end sequences were obtained using a NextSeq
859 500 sequencer (Illumina). *Data analyses:* Data was analyzed by following the ENCODE Kundaje

860 lab ATAC-seq pipeline (https://www.encodeproject.org/pipelines/ENCPL792NWO/).
861 Sequences were trimmed using Trimmomatic [75] and aligned on the Mus musculus genome
862 assembly mm10 using Bowtie2 [76]. After filtering out low quality, multiple mapped,
863 mitochondrial, and duplicated reads using SAMtools [77] and the Picard Toolkit
864 (http://broadinstitute.github.io/picard/), fragments with map length ≤ 146 bp were kept as
865 nucleosome-free fraction. Genomic loci targeted by TDE1 were defined as 38-bp regions
866 centered either 4 (plus strand reads) or 5-bp (negative strand reads) downstream of the
867 read's 5'-end. ATAC-seq peaks were called using the MACS2 software (narrowPeak; q-value
868 ≤ 0.01) [38]. FRiP scores were calculated as the fraction of TDE1 targeted loci falling into the
869 called peaks. Overlapping peaks across samples were merged and annotated for the
870 occurrence of TF binding motifs of interest (Suppl. Table 11) and the closest gene using Homer
871 [38]. TDE1 targeted loci overlapping the merged peaks were extracted and converted to a
872 bedgraph file with a scaling factor to one million reads using BEDTools [78], and further to tdf
873 format to visualize peaks on the Integrative Genomics Viewer [79]. The total number of TDE1
874 targeted loci overlapping the merged peaks were counted using BEDOPS [80], normalized for
875 peak lengths and a sequencing depth with per one million scaling factor, standardized and
876 used for hierarchical cluster analysis using R hclust [81] and gplots (https://CRAN.R-
877 project.org/package=gplots). The detailed analysis pipeline is provided in the
878 ATAC_seq_analysis_pipeline.docx file. The overall mapping rate with Bowtie2 averaged
879 98.6%, the mapping rate to the mitochondrial genome 4.1%, the duplicate fragment rate
880 6.0%, the proportion of usable reads after filtration 83.4%, and the FRiP score 34.1%. The
881 FRiP score was significantly lower for E13 samples (reminiscent of the E14.5 samples in [82]),
882 yet not so in the equivalent DD13 samples (Suppl. Table 16).
883 ***Accessing publicly available scATAC-Seq and bulk ATAC-seq.*** Single-cell ATAC-seq data from
884 8-wk wild-type C57BL/6 mouse retinas were obtained from GEO:GSE164044 [39] and
885 analyzed using Cell Ranger ATAC v1.2.0 and Loupe Browser v5.0 with default settings (10X
886 Genomics). Bulk ATAC-seq data on FACS-sorted rod and cone photoreceptors from 8-wk Nrl-
887 eGFP and Opn1mw-GFP mouse, respectively, were obtained from GEO:GSE83312 [83] and
888 analyzed as above.
889 ***Downstream analyses***. *Width of developmental trajectories in 2D UMPA space:* To test
890 whether the developmental trajectories were more tightly regulated in NaR than in 3D-RA we
891 computed the average distance (computed as the Euclidian distance in 2D-UMAP space,

892 i.e.$\sqrt{(x_1 - x_2)^2 + (y_1 - y_2)^2}$) between 500 randomly selected NaR and 500 randomly
893 selected 3D-RA cells and their n nearest neighbors (with n ranging from 1 to 50). The number
894 of cells per developmental stage was adjusted between NaR and 3D-RA by down sampling to
895 the number of the least populated source. The corresponding calculations were performed
896 five times. The curves shown in Fig. 2D correspond to the averages across the five replicates.
897 The grey confidence zone in Fig. 2D is bounded by the maxima and minima across the five
898 replicates. The corresponding script was written in Perl (Dev_path_width.pl) and the graph
899 generated in R (Path_width.R). *Within developmental stage cell type entropy:* To compare
900 cell type diversity within developmental stage between NaR and 3D-RA, we first equalized the
901 number of cells with developmental stage between NaR and 3D-RA by randomly dropping
902 cells from the most populated source. We then sampled two cells within cell source (NaR and
903 3D-RA) and developmental stage and checked whether they were from the same cell type or
904 not. This was repeated 1,000 times yielding a measure of cell type diversity akin to (1-
905 entropy). Down-sampling of cells was repeated 100 times. Each data point in Fig. 2E
906 corresponds to (1-Entropy) for one such random sample. The corresponding script was
907 written in Perl (entropy.pl) and the graph generated in R (Entropy.R). *Differential expression*
908 *analyses:* Differential expression analyses to identify genes that are upregulated in specific
909 cell types when compared to all other ones (Cell type > Others) or that are differentially
910 expressed between NaR and 3D-RA in a given cell type (Nar > 3D-RA and 3D-RA > NaR) were
911 performed with the *Findmarkers* function in Seurat (https://satijalab.org/seurat/). *Pathway*
912 *analyses:* Pathway enrichment analyses were conducted using the on-line Reactome analysis
913 tools [33,34]. Mouse gene identifiers were converted to human counterparts. Pathway
914 analysis results were downloaded as flat files. A total of 392 pathways with enrichment p-
915 value ≤ 0.01 in at least one analysis were kept and manually sorted according to Reactome
916 hierarchy (Man_processed_reactome_output.txt). A pathway is enriched in a list of genes if
917 it contains more components of the pathway than expected by chance (given the number of
918 genes in the list). The overlapping genes ("Found entities") hence define the enrichment.
919 The same pathway can be enriched in two gene lists due to the same, distinct or partially
920 overlapping sets of "found entities". We quantified the degree of overlap between sets of
921 "found entities" for the 1,313 pathway enrichments using principal component (PC) analysis
922 in a space defined by the presence/absence of 1,335 genes. The distance between sets of

923 "found entities" in a space consisting of the 20 first PCs was projected in 3D space using t-
924 distributed stochastic neighbor embedding (tSNE) implemented with the *Rtsne* R function.
925 3D tSNE coordinates were converted to hexadecimal RGB code and used to color the sets of
926 "found entities" (corresponding to the enrichment of a pathway in a specific gene list) when
927 generating 2D tSNE graphs (SFig. 4), or when generating a tile showing the pathways enriched
928 in specific analyses (Cell type>OTHER, NaR > 3D-RA or 3D-RA > NaR) and cell type within
929 analysis (NE, RPE, ERPC, LRPC, NRPC, RGC, HC, AC, PRP, C, R, BC or MC) (Fig. 3B). The
930 corresponding scripts were written in Perl (Reactome_analysis.pl) and R
931 (Reactome_analysis.R). *Identifying regulatory toggles:* We used Homer [38] to compile the
932 number of occurrences of 336 binding motifs for 151 of 307 dynamically regulated TF in
933 98,181 ATAC-Seq peaks assigned to 19,170 genes. For each gene, the data were summarized
934 as (i) the total number of occurrences, and (ii) the mean number of occurrences per peak (i.e.
935 density), for each of the 336 binding motifs (STable 11). We then checked - for each of the
936 336 binding motifs separately - whether the number ("total" in STable 11) and density
937 ("mean" in STable 11) of motifs differed significantly between genes that were upregulated
938 versus downregulated in every one of the 13 cell types. Differential expression analyses to
939 identify genes that are up- and downregulated in specific cell types were performed with the
940 *Findmarkers* function in Seurat (https://satijalab.org/seurat/). The corresponding results are
941 summarized in a series of files labelled, respectively, "NaR/RET_<CELL_TYPE>_markers.txt"
942 for NaR, and "3D_RA/IPS_<CELL_TYPE>_markers.txt" for 3D_RA. We used a threshold q-
943 value of 0.05 to declare a gene as significantly up- or down-regulated in a given cell type. The
944 statistical significance of the difference in number and density of binding motifs between up-
945 and down-regulated genes was computed using Wilcoxon rank-based test implemented with
946 the wilcox.test R function. Differences were deemed significant if the q-value (computed
947 with the qvalue R function) was ≤ 0.01. Corresponding results are provided as STable 13 for
948 NaR and STable 14 for 3D-RA. The graphs for figure 5 were generated using the
949 Comb_scRNA_ATAC_seq R script.
950 All used scripts and datasets are available without restrictions from:
951 http://web.giga.ulg.ac.be/pubdata/UAG/Georges_A_2020.
952
953 **AUTHOR CONTRIBUTIONS**

954 Conceived and designed the experiments: AG, MT, MM, HT, MG. Performed the experiments:
955 AG, HT, FL, LK, SD. Analyzed the data: AG, AL, HT, MS, LD, MG. Contributed
956 reagents/materials/analysis tools/supervision: AG, AL, LN, JMR, LD, MS, MT, MG. Wrote the
957 paper: AG, HT, MG.
958

959 **ACKNOWLEDGEMENTS**

960 We are grateful to Tomoyo Hashiguchi for teaching the 3D-RA culture protocol and to
961 Tomohiro Masuda and Akishi Onishi for their comments and suggestions. We thank the GIGA
962 Genomics platform for their help both with scRNA-seq experiments and early bio-informatic
963 analyses (especially Wouter Coppieters and Benoit Charloteaux). We are grateful to Vincent
964 Lambert for assisting with the dissection of NaR. This work was financially supported by the
965 "King Baudouin Foundation", the "Global Ophthalmology Awards Program (GOAP) from
966 Bayer", and the "Fonds Leon Fredericq". LD and LN are respectively postdoctoral researcher
967 and senior associate researcher of the FRS-FNRS. We are grateful to the Dyer laboratory for
968 the scATAC-Seq data.
969

970 **DATA AVAILABILITY**

971 All data generated as part of this work are available without restrictions. They have been
972 deposited under accession numbers E-MTAB-9440 and E-MTAB-9395. All data and analysis
973 pipelines are available at http://web.giga.ulg.ac.be/pubdata/UAG/Georges_A_2020. The
974 authors declare that they have no competing interests.
975

976 **ETHICAL APPROVAL**

977 Ethical approval: All animal procedures were approved by the Animal Ethics Committee at
978 University of Liège (approval no. 17-1908) and performed in accordance with the Guide for
979 the Care and Use of Laboratory Animals at University of Liège.
980

981 **REFERENCES**

982 1. Eiraku M, Takata N, Ishibashi H, Kawada M, Sakakura E, Okuda S, Sekiguchi K, Adachi T,
983 Sasai Y. Self-organizing optic-cup morphogenesis in three-dimentional culture. Nature.
984 2011; 472:51-56.

985 2. Meyer JS, Howden SE, Wallace KA, Verhoeven AD, Wright LS, Capowski EE, Pinilla I, Martin
986 JM, Tian S, Stewart R, et al. Optic vesicle-like structures derived from human pluripotent
987 stem cells facilitate a customized approach to retinal disease treatment. Stem Cells. 2011;
988 29:1206-1218.
989 3. Nakano T, Ando S, Takata N, Kawada M, Muguruma K, Sekiguchi K, Saito K, Yonemura
990 S, Eiraku M, Sasai Y. Self-formation of optic cups and storable stratified neural retina
991 from human ES cells. Cell Stem Cell. 2012;10: 771–785.
992 4. Li JQ, Welchowski T, Schmid M, Letow J, Wolpers AC, Holz FG, Finger RP. Retinal
993 diseases in Europe. Euretina Whitebook 2017;
994 https://www.euretina.org/downloads/EURETINA_Retinal_Diseases.pdf.
995 5. Jin ZB, Okamoto S, Osakada F, Homma K, Assawachananont J, Hirami Y, Iwata T, Takahashi
996 M. Modeling retinal degeneration using patient-specific induced pluripotent stem cells.
997 PLoS One. 2011;6:e17084.
998 6. Achberger K, Haderspeck JC, Kleger A, Liebau S. Stem cell-based retina models. Advanced
999 Drug Delivary Reviews. 2019; 140:33-50.
1000 7. Völkner M, Zschätzsch M, Rostovskaya M, Overall RW, Busskamp V, Anastassiadis K, Karl
1001 MO. Retinal organoid from pluripotent stem cells efficiently recapitulate retinogenesis.
1002 Stem Cells Rep. 2016;6: 525-538.
1003 8. Shekhar K, Lapan SW, Whitney IE, Tran NM, Macosko EZ, Kowalczyk M, Adiconis X, Levin
1004 JZ, Nemesh J, Goldman M, McCarroll SA, Cepko CL, Regev A, Sanes JR. Comprehensive
1005 classification of retinal bipolar neurons by single-cell transcriptomics. Cell. 2016;166:
1006 1308-1323.
1007 9. Saelens W, Cannoodt R, Todorov H & Saeys Y. A comparison of single cell trajectory
1008 inference methods. Nat Biotechnol. 2019;37: 547–554.
1009 10. Haghverdi L, Büttner M, Wolf FA, Buettner F, Theis FJ. Diffusion pseudotime robustly
1010 reconstructs lineage branching. Nat Methods 2016;13:845-848.
1011 11. La Manno G, Soldatov R, Zeisel A, Braun E, Hochgerner H, Petukhov V, Lidschreiber K,
1012 Kastriti ME, Lonnerberg P, Furlan A, Fan J, Borm LE, Liu Z, Van Bruggen D, Guo J, He X,
1013 Barker R, Sundstrom E, Castelo-Branco G, Cramer P, Adameyko I, Linnarsson S,
1014 Kharchenko P. RNA velocity of single cells. Nature. 2018;560: 494-510.
1015 12. Bergen V, Lange M, Peidli S, Wolf FA, Theis FJ. Generalizing RNA velocity to transient cell
1016 states through dynamic modeling. Nat Biotechnol. 2020; 38: 1408-1414.

1017 13. Camara PG. Methods and challenges in the analysis of single-cell RNA-sequencing data.
1018 Curr Opin Syst Biol. 2018; 7:47-53.
1019 14. Trapnell C, Cacchiarelli D, Grimsby J, Pokharel P, Li S, Morse M, Lennon NJ, Livak KJ,
1020 Mikkelsen TS, Rinn JL. The dynamics and regulators of cell fate decisions are revealed by
1021 pseudotemporal ordering of single cells. Nat Biotechnol. 2014;32:381-386.
1022 15. Collin J, Queen R, Zerti D, Dorgau B, Hussain R, Coxhead J, Cockell S, Lako M.
1023 Deconstructing retinal organoids: single cell RNA-Seq reveals the cellular components of
1024 human pluripotent stem cell-derived retina. Stem Cells. 2019;37: 593-598.
1025 16. Sridhar A, Hoshino A, Finkbeiner CR, Chitsazan A, Dai L, Haugan AK, Eschenbacher KM,
1026 Jackson DL, Trapnell C, Bermingham-McDonogh O, Glass I, Reh TA. Single Cell
1027 Transcriptomic Comparison of human fetal retina, hPSC-derived retinal organoids, and
1028 long-term retinal cultures. Cell Rep. 2020;30:1644-1659.
1029 17. Cowan CS, Renner M, De Gennaro M, Gross-Scherf B, Goldblum D, Hou Y, Munz
1030 M, Rodrigues TM, Krol J, Szikra T, Cuttat R, Waldt A, Papasaikas P, Diggelmann
1031 R, Patino-Alvarez CP, Galliker P, Spirig SE, Pavlinic D, Gerber-Hollbach N, Schuierer
1032 S, Srdanovic A, Balogh M, Panero R, Kusnyerik A, Szabo A, Stadler MB, Orgül S, Picelli
1033 S, Hasler PW, Hierlemann A, Scholl HPN, Roma G, Nigsch F, Roska B. Cell types of the
1034 human retina and its organoids at single-cell resolution. Cell. 2020;182:1623-1640.
1035 18. Yan F, Powell DR, Curtis D & Wong NC. From reads to insight: a hitchhiker's guide to ATAC-
1036 Seq data analysis. Genome Biol. 2020;21: 22.
1037 19. Gonzalez-Cordero A, West EL, Pearson RA, Duran Y, Carvalho LS, Chu CJ, Naeem A,
1038 Blackford SJ, Georgiadis A, Lakowski J, Hubank M, Smith AJ, Bainbridge JWB, Sowden JC,
1039 Ali RR. Photoreceptor precursors derived from three-dimensional embryonic stem cell
1040 cultures integrate and mature within adult degenerate retina. Nat Biotechnol. 2013;31:
1041 741- 747.
1042 20. Akimoto M, Cheng H, Zhu D, Brzezinski JA, Khanna R, Filippova E, C T Oh E, Jing Y, Linares
1043 JL, Brooks M, Zareparsi S, Mears AJ, Hero A, Glaser T, Swaroop A. Targeting of GFP to
1044 newborn rods by Nrl promoter and temporal expression profiling of flow-sorted
1045 photoreceptors. Proc Natl Acad Sci USA. 2006;103: 3890-3895.
1046 21. Eiraku M, Sasai Y. Mouse embryonic stem cell culture for generation of three-dimensional
1047 retinal and cortical tissues. Nat Prot. 2012;7: 69–79.

1048 22. Assawachananont J, Mandai M, Okamoto S, Yamada C, Eiraku M, Yonemura S, Sasai Y,
1049 Takahashi M. Transplantation of embryonic and induced pluripotent stem cell-derived
1050 3D retinal sheets into retinal degenerative mice. Stem Cell Rep. 2014;2: 662–674.
1051 23. Butler A, Hoffman P, Smibert P, Papalexi E, Satija R. Integrating single-cell transcriptomic
1052 data across different conditions, technologies, and species. Nat Biotech. 2018;36: 411-
1053 420.
1054 24. McInnes L, Healy J, Melville J. UMAP: Uniform Manifold Approximation and Projection. J.
1055 Open Source Software. 2018;3: 861.
1056 25. Clark BS, Stein-O'-Brien GL, Shiau F, Cannon GH, Davis-Marcisak E, Sherman T, Santiago
1057 CP, Hoang TV, Rajaii F, James-Esposito RE, Gronostajski RM, Fertig EJ, Goff LA, Blackshaw
1058 S. Comprehensive analysis of retinal development at single cell resolution identifies NFI
1059 factors as essential for mitotic exit and specification of late-born cells. Neuron. 2019;102:
1060 1111-1126.
1061 26. Tiroshi I, Izar B, Prakadan SM, Wadsworth MH, Treacy D, Trombetta JJ, Rotem A, C
1062 Rodman, Lian C, Murphy G, Fallahi-Sichani M,Dutton-Regester K, Lin JR, Cohen O, Shah P,
1063 Lu D, Genshaft A, Hughes TK, Ziegler CGK, Kazer SW, Gaillard A, Kolb KE, Villani AC,
1064 Johannessen CM, Andreev AY, Van Allen EM, Bertagnolli M, Sorger PK, Sullivan RJ,Flaherty
1065 RT,Frederick DT, Jané-Valbuena J, Yoon CH, Rozenblatt-Rosen O, Shalek AK, Regev A,
1066 Garraway LA. Dissecting the multicellular ecosystem of metatastic melanoma by single-
1067 cell RNA-seq. Science. 2016;352:189-196.
1068 27. Trimarchi JM, Cho SH, Cepko CL. Identification of genes expressed preferentially in the
1069 developing peripheral margin of the optic cup. Dev Dyn. 2009;238: 2327.
1070 28. Liu J, Reggiani JDS, Laboulaye ME, Pandey S, Chen B, Rubenstein JLR, Krishnaswamy A,
1071 Sanes JR. Tbr1 instructs laminar pattering of retinal ganglion cell dendrites. Nat Neurosci.
1072 2018;21: 659-670.
1073 29. Yan W, Laboulaye MA, Tran NM, Whitney IE, Benhar I, Sanes JR. Mouse retinal cell atlas:
1074 molecular identification of over sixty amacrine cell types. J. Neurosci. 2020;40: 5177-5195.
1075 30. Bassett EA, Wallace VA. Cell fate determination in the vertebrate retina. Trends in
1076 Neurosciences. 2012; 35:565-573.
1077 31. Reese B. Development of the retina and optic pathway. Vision Res. 2011;51: 613–632.
1078 32. Kuwahara A, Ozone C, Nakano T, Saito K, Eiraku M, Sasai Y. Generation of a ciliary margin-
1079 like stem cell niche from self-organizing human retinal tissue. Nat Commun. 2015;6:6286.

1080 33. Fabregat A, Jupe S, Matthews L, Sidiropoulos K, Gillespie M, Garapati P, Haw R, Jassal B,
1081 Korninger F, May B, Milacic M, Roca CD, Rothfels K, Sevilla C, Shamovsky V, Shorser S,
1082 Varusai T, Viteri G, Weiser J, Wu G, Stein L, Hermjakob H, D'Eustachio P. The reactome
1083 pathway knowledgebase. Nucl Ac Res. 2018 ;44: D481-487.
1084 34. Jassal B, Matthews L, Viteri G, Gong C, Lorente P, Fabregat A, Sidiropoulos K, Cook J,
1085 Gillespie M, Haw R, Loney F, May B, Milacic M, Rothfels K, Sevilla C, Shamovsky V, Shorser
1086 S, Varusai T, Weiser J, Wu G, Stein L, Hermjakob H, D'Eustachio P. The reactome pathway
1087 knowledgebase. Nucleic Acids Res. 2020;48: D498-D503.
1088 35. Kanamori M, Konno H, Osato N, Kawai J, Hayashizaki Y, Suzuki H. A genome-wide and
1089 nonredundant mouse transcription factor database. Biochem Biophys Res Commun.
1090 2004;322:787-793.
1091 36. Corces MR, Trevino AE, Hamilton EG, Greenside PG, Sinnott-Armstrong NA, Vesuna S,
1092 Satpathy AT, Rubin AJ, Montine KS, Wu B, Kathiria A, Cho SW, Mumbach MR, Carter AC,
1093 Kasowski M, Orloff LA, Risca VI, Kundaje A, Khavari PA, Montine TJ, Greenleaf WJ & Chang
1094 HY. An improved ATAC-seq protocol reduces background and enables interrogation of
1095 frozen tissues. Nat Methods. 2017;14:959-962.
1096 37. Zhang Y, Liu T, Meyer CA, Eeckhoute J, Johnson DS, Bernstein BE, Nusbaum C, Myers RM,
1097 Brown M, Li W & Liu XS. Model-based analysis of ChIP-Seq (MACS). Genome Biol.
1098 2008;9:R137.
1099 38. Heinz S, Benner C, span N, Bertolino E, Lin YC, Laslo P, cheng JX, Murre C, Singh H, Glass
1100 CK. Simple combinations of lineage-determining transcription factors prime cis-regulatory
1101 elements required for macrophage and B cell identities. Mol Cell. 2010; 38:576-589.
1102 39. Norrie JL, Lupo MS, Xu B, Al Diri I, Valentine M, Putnam D, Griffiths L, Zhang J, Johnson D,
1103 Easton J, Shao Y, Honnell V, Frase S, Miller S, Stewart V, Zhou X, Chen X, Dyer MA.
1104 Nucleosome dynamics during retinal development. Neuron. 2019; 104: 512-528.
1105 40. Brooks MJ, Chen HY, Kelley RA, Mondal AK, Nagashima K, De Val N, Li T, Chaitankar V,
1106 Swaroop A. Improved retinal organoid differentiation by modulating signaling pathways
1107 revealed by comparative transcriptome analyses with development in vivo. Stem Cell
1108 Reports. 2019; 13:891-905.
1109 41. Swaroop A, Kim D, Forrest D. Transcriptional regulation of photoreceptor development
1110 and homeostasis in the mammalian retina. Nat Rev Neurosc. 2010; 11:563-576.

1111 42. Brzezinski JA, Reh TA. Photoreceptor cell fate specification in vertebrates. Development.
1112 2015; 142: 3263-3273.
1113 43. Buono L, Martinze-Morales J-R. Retina development in vertebrates: systems biology
1114 approaches to understanding genetic programs. Bioessays. 2020; 42: e1900187.
1115 44. Smith SG, Haynes KA, Hegde AN. Degradation of transcriptional repressor ATF4 during
1116 long-term synaptic plasticity. Int J Mol Sci. 2020; 21: 8543.
1117 45. Sena E, Rocques N, Borday C, Amin HSM,Parain K, Sitbon D, Chesneau A, Durand BC.
1118 Barhl2 maintains T cell factors as repressors and thereby switches off the Wnt/β-catenin
1119 response driving Spemann organizer formation. Development. 2019; 146: dev.173112.
1120 46. Reig G, Cabrejos ME, Concha ML. Functions of BarH transcription factors during
1121 embryonic development. Dev Biol. 2007; 302: 367-375.
1122 47. Bauer DE, Orkin SH. Hemoglobin switching's surprise: the versatile transcription factor
1123 BCL11A is a master repressor of fetal hemoglobin. Curr Opin Genet Dev. 2015; 33: 62-70.
1124 48. https://www.uniprot.org/uniprot/Q9H334
1125 49. Sollis E, Graham SA, Vino A, Froehlich H, Vreeburg M, Dimitropoulou D, Gilissen C, Pfundt
1126 R, Rappold GA, Brunner HG, Deriziotis P, Fisher SE. Identification and functional
1127 characterization of de novo FOXP1 variants provides novel insights into the etiology of
1128 neurodevelopmental disorder. Hum Mol Genet. 2016; 25: 546-557.
1129 50. https://www.uniprot.org/uniprot/O15409
1130 51. https://www.uniprot.org/uniprot/Q9UBP5
1131 52. Nakagawa O, McFadden DG, Nakagawa M, Yanagisawa H, Hu T, Srivastava D, Olsen EN.
1132 Members of the HRT family of basic helix-loop-helix proteins act as transcriptional
1133 repressors downstream of Notch signaling. Proc Natl Acad Sci USA. 2000; 97: 13655-
1134 13660.
1135 53. Nakakura EK, Watkins DN, Schuebel KE, Sriuanpong V, Borges MW, Nelkin BD, Ball DW.
1136 Mammalian Scratch: a neural-specific Snail family transcriptional repressor. Proc Natl
1137 Acad Sci USA. 2001; 98: 4010-4015.
1138 54. Li X, Perissi V, Liu F, Rose DW, Rosenfeld MG. Tissue-specific regulation of retinal and
1139 pituitary precursor cell proliferation. Science. 2002; 297: 1180-1183.
1140 55. Liu Y-R, Laghari ZA, Novoa CA, Hughes J, Webster JRM, Goodwin PE, Wheatley SP, Scotting
1141 PJ. Sox2 acts as a transcriptional repressor in neural stem cells. BMC Neurosci. 2014; 15:
1142 95.

1143 56. Melhuish TA, Taniguchi K, Wotton D. Tgif1 and Tgif2 regulate axial patterning in mouse.
1144 PLoS ONE. 2016; 11: e0155837.
1145 57. Dorval KM, Bobechko BP, Ahmad KF, Bremmer R. Transcriptional activity of the paired-
1146 like homeodomain proteins CHX10 and VSX1. J Biol Chem. 2005; 280: 10100-10108.
1147 58. Vitorino M, Jusuf PR, Maurus D, Kimura Y, Higashijima S-I, Harris WA. Vsx2 in the zebrafish
1148 retina: restricted lineages through derepression. Neural Dev. 2009; 4:14.
1149 59. https://www.uniprot.org/uniprot/O60315
1150 60. Siggs OM, Beutler B. the BTB-ZF transcription factors. Cell Cycle. 2012; 11: 3358-3369.
1151 61. Zaret KS, Carroll JS. Pioneer transcription factors: establishing competence for gene
1152 expression. Genes & Dev. 2011; 25: 2227-2241.
1153 62. Morris SA. Direct lineage reprogramming via pioneer factors; a detour through
1154 developmental gene regulatory networks. Development. 2016; 143: 2696-2705.
1155 63. Raposo AASF, Vasconcelos FF, Drechsel D, Marie C, Johnston C, Dolle D, Bithell A, Gillotin
1156 S, van den Berg DLC, Ettwiller L, Flicek P, Crawford GE, Parras CM, Berninger B, Buckley
1157 NJ, Guillemot F, Castro DS. Ascl1 coordinately regulates gene expression and the
1158 chromatin landscape during neurogenesis. Cell Reports. 2015; 10: 1544-1556.
1159 64. Gao R, Liang X, Cheedipudi S, Cordero J, Jiang X, Zhang Q, Caputo L, Günther S, Kuenne C,
1160 Ren Y, Bhattacharya S, Yuan X, Barreto G, Chen Y, Braun T, Evans SM, Sun Y, Dobreva G.
1161 Pioneering function of Isl1 in the epigenetic control of cardiomyocyte fate. Cell Research.
1162 2019; 29: 486-501.
1163 65. Gargaro M, Scalisi G, Manni G, Mondanelli G, Grohmann U, Fallarino F. The landscape of
1164 Ahr regulators and coregulators to fine-tune Ahr functions. Int J Mol Sci. 2021; 22: 757
1165 66. Filtz TM, Vogel WK, Leid M. Regulation of transcription factor activity by interconnected,
1166 post-translational modifications. Trends Pharmacol Sci. 2014;35: 76-85.
1167 67. Lambert SA, Jolma A, Campitelli LF, Das PK, Yin Y, Albu M, Chen X, Taipale J, Hughes TR,
1168 Weirauch MT. The human transcription factors. Cell. 2018;172: 650-665.
1169 68. White MA, Kwasnieski JC, Myers CA, Shen SQ, Corbo JC, Cohen BA. A simple grammar
1170 defines activating and repressing cis-regulatory elements in photoreceptors. Cell Reports.
1171 2016; 17: 1247-1254.
1172 69. Dixit A, Parnas O, Li B, Fulco CP, Jerby-Arnon L, Marjanovic ND, Dionne D, Burks T,
1173 Raychowdhury R, Adamson B, Norman TM, Lander ES, Weissman JS, Friedman N, Regev

1174 A. Perturb-Seq: dissecting molecular circuits with scalable single-cell RNA profiling of
1175 pooled genetic screens. Cell. 2016;167: 1853-1866.
1176 70. Homma K, Okamoto S, Mandai M, Gotoh N, Rajasimha HK, Chang YS, Chen S, Cogliati T,
1177 Swaroop A, Takahashi M. Developing rods transplanted into the degenerating retina of
1178 Crx-knockout mice exhibit neural activity similar to native photoreceptors. Stem Cells.
1179 2013;31:1149–1159.
1180 71. Iwasaki Y, Sugita S, Mandai M, Yonemura S, Onishi A, Ito SI, Mochizuki M, Ohno-Matsui K,
1181 Takahashi M. Differentiation/purification protocol for retinal pigment epithelium from
1182 mouse induced pluripotent stem cells as a research tool. PLoS One. 2016;11: 1–20.
1183 72. Eiraku M, Takata N, Ishibashi H, Kawada M, Sakakura E, Okuda S, Sekiguchi K, Adachi T &
1184 Sasai Y. Self-organizing optic-cup morphogenesis in 3D culture. Nature. 2011;472: 51-56.
1185 73. Osakada F, Ikeda H, Mandai M, Wataya T, Watanabe K, Yoshimura N, Akaike A, Sasai Y &
1186 Takahashi M. Toward the generation of rod and cone photoreceptors from mouse,
1187 monkey and human embryonic stem cells. Nat Biotechnol. 2008;26: 215–224.
1188 74. Macosko EZ, Basu A, Satija R, Nemesh J, Shekhar K, Goldman M, Tirosh I, Bialas AR,
1189 Kamitaki N, Martersteck, Trombetta JJ, Weitz DA, Sanes JR, Shalek AK, Regev A, McCarroll
1190 SA. Highly parallel genome wide expression profiling of individual cells using nanoliter
1191 droplets. Cell. 2015;161: 1202:1214.
1192 75. Bolger AM, Lohse M, Usadel B. Trimmomatic: a flexible trimmer for Illumina sequence
1193 data. Bioinformatics. 2014; 30: 2114-2120.
1194 76. Langmead A, Salzberg S. Fast gapped-read alignment with Bowtie 2. Nature Methods.
1195 2012 ; 9 : 357-359.
1196 77. Li H, Handsaker B, Wysoker A, Fennell T, Ruan J, Homer N, Marth G, Abecasis G, Durbin R.
1197 1000 Genome Project Data Processing Subgroup. The Sequence Alignment/Map format
1198 and SAMtools. Bioinformatics. 2009;25: 2078-2079.
1199 78. Quinlan AR & Hall IM. BEDTools: a flexible suite of utilities for comparing genomic
1200 features. Bioinformatics. 2010;26: 841-842.
1201 79. Robinson JT, Thorvaldsdottir H, Winckler W, Guttman M, Lander ES, Getz G & Mesirov JP.
1202 Integrative genomics viewer. Nat Biotechnol. 2011;29:24-26.
1203 80. Neph S, Kuehn MS, Reynolds AP, Haugen E, Thurman RE, Johnson AK, Rynes E, Maurano
1204 MT, Vierstra J, Thomas S, Sandstrom R, Humbert R, Stamatoyannopoulos JA. BEDOPS: high
1205 performance genomic feature operations. Bioinformatics. 2012;28: 1919-1920.

1206 81. Murtagh F, Legendre P. Ward's hierarchical agglomerative clustering method: which
1207 algorithms implement Ward's criterion ? J Classification. 2014;31:274-295.
1208 82. Aldiri I, Xi B, Wang L, Chan X, Hiler D, Griggiths L, Valentine M, Shirinifard A, Thiagarajan
1209 S, Sablauer A, Barabas M-E, Zhang J, Johnson D, Frase S, Zhou X, Easton J, Zhang J, Maris
1210 ER, Wilson RK, Downing JR, Dyer MA. The dynamic epigenetic landscape of the retine
1211 during development, reprogramming and tumorigenesis. Neuron. 2017. 94: 550-568.
1212 83. Hughes AE, Enright JM, Myers CA, Shen SQ, et al. Cell type-specific epigenomic analysis
1213 reveals a uniquely closed chromatin architecture in mouse rod photoreceptors. Sci Rep.
1214 2017; 7: 43184.
1215